

# Opposing roles for p16<sup>Ink4a</sup> and p19<sup>Arf</sup> in senescence and ageing caused by BubR1 insufficiency

Darren J. Baker<sup>1</sup>, Carmen Perez-Terzic<sup>2</sup>, Fang Jin<sup>1</sup>, Kevin Pitel<sup>1</sup>, Nicolas J. Niederländer<sup>3</sup>, Karthik Jeganathan<sup>1</sup>, Satsuki Yamada<sup>3</sup>, Santiago Reyes<sup>3</sup>, Lois Rowe<sup>3</sup>, H. Jay Hiddinga<sup>4</sup>, Norman L. Eberhardt<sup>4</sup>, Andre Terzic<sup>3</sup> and Jan M. van Deursen<sup>1,4,5</sup>

Expression of p16<sup>Ink4a</sup> and p19<sup>Arf</sup> increases with age in both rodent and human tissues. However, whether these tumour suppressors are effectors of ageing remains unclear, mainly because knockout mice lacking p16<sup>Ink4a</sup> or p19<sup>Arf</sup> die early of tumours. Here, we show that skeletal muscle and fat, two tissues that develop early ageing-associated phenotypes in response to BubR1 insufficiency, have high levels of p16<sup>Ink4a</sup> and p19<sup>Arf</sup>. Inactivation of p16<sup>Ink4a</sup> in BubR1-insufficient mice attenuates both cellular senescence and premature ageing in these tissues. Conversely, p19<sup>Arf</sup> inactivation exacerbates senescence and ageing in BubR1 mutant mice. Thus, we identify BubR1 insufficiency as a trigger for activation of the *Cdkn2a* locus in certain mouse tissues, and demonstrate that p16<sup>Ink4a</sup> is an effector and p19<sup>Arf</sup> an attenuator of senescence and ageing in these tissues.

Cellular senescence is a state of irreversible growth arrest that can be induced by various cellular stressors<sup>1,2</sup>. The *Cdkn2a* locus encodes two separate tumour suppressors, p16<sup>Ink4a</sup> (A001711), a cyclin-dependent kinase (Cdk) inhibitor that can block G<sub>1</sub>-S progression when present above a certain level, and p19<sup>Arf</sup> (A001713), a positive regulator of the transcription factor p53 that integrates and responds to a wide variety of cellular stresses<sup>1,3-5</sup>. Both p16<sup>Ink4a</sup> and p19<sup>Arf</sup> are effectors of senescence in cultured cells<sup>6</sup> and their levels increase with ageing in many tissues<sup>7,8</sup>. This has led to speculation that their induction is causally implicated in *in vivo* senescence and organismal ageing. However, rigorous testing of this notion has been difficult because mice that lack p16<sup>Ink4a</sup> or p19<sup>Arf</sup> die of cancer long before they reach the age at which normal mice start to develop age-related disorders<sup>1,2</sup>. Recent evidence in middle-aged p16<sup>Ink4a</sup> knockout mice indicates that the age-induced expression of p16<sup>Ink4a</sup> limits the proliferative and regenerative capacity of progenitor populations<sup>9-11</sup>. Yet, whether the increased stem-cell proliferation and tissue regeneration seen in p16<sup>Ink4a</sup> knockouts actually delay onset of age-related pathologies remains unknown because of the limited animal lifespan<sup>1,12</sup>.

One approach to study the role of p16<sup>Ink4a</sup> and p19<sup>Arf</sup> in ageing would be to determine whether their respective inactivation by single gene mutations, in mouse models that develop ageing-associated pathologies at an early age, would prevent or delay premature ageing. Mutant mice with low levels of the mitotic checkpoint protein BubR1 (called BubR1 hypomorphic or *BubR1*<sup>HH</sup> mice, A003172) undergo premature separation of sister chromosomes and develop progressive aneuploidy along

with various progeroid phenotypes that include short lifespan, cachectic dwarfism, lordokyphosis (abnormal curvature of the spine), sarcopaenia (age-related skeletal muscle atrophy), cataracts, craniofacial dysmorphisms, arterial stiffening, loss of (subcutaneous) fat, reduced stress tolerance and impaired wound healing<sup>13-15</sup>. During the course of natural ageing, several mouse tissues show a marked decline in BubR1 protein expression, which, combined with the observation that *BubR1*<sup>HH</sup> mice age prematurely, suggests a possible role for BubR1 in regulating natural ageing<sup>13-15</sup>. Here we show that certain mouse tissues induce p16<sup>Ink4a</sup> and p19<sup>Arf</sup> in response to BubR1 hypomorphism. Using *BubR1*<sup>HH</sup> mice in which these tumour suppressors are lacking, we have demonstrated that p16<sup>Ink4a</sup> is an effector of cellular senescence and ageing, whereas, p19<sup>Arf</sup> acts to suppress cellular senescence and ageing.

## RESULTS

### p16<sup>Ink4a</sup> inactivation increases the lifespan of *BubR1*<sup>HH</sup> mice

To determine the requirement for p16<sup>Ink4a</sup> in the development of progeroid phenotypes in BubR1-insufficient mice, we bred *BubR1*<sup>HH</sup> mice on a p16<sup>Ink4a</sup> homozygous-null genetic background. In total, 86 *BubR1*<sup>HH</sup>, p16<sup>Ink4a</sup><sup>-/-</sup>, 192 *BubR1*<sup>HH</sup>, 160 *BubR1*<sup>+/+</sup> and 44 p16<sup>Ink4a</sup><sup>-/-</sup> mice were generated and monitored for development of age-related phenotypes for a period of one year. Inactivation of p16<sup>Ink4a</sup> extended the lifespan of *BubR1*<sup>HH</sup> mice by 25% (Fig. 1a). Although the median lifespan of *BubR1*<sup>HH</sup> mice was extended in the absence of p16<sup>Ink4a</sup>, the maximum lifespan was not, suggesting that the condition(s) that cause(s) death was not rescued by p16<sup>Ink4a</sup> inactivation.

<sup>1</sup>Department of Pediatric and Adolescent Medicine, <sup>2</sup>Department of Physical Medicine and Rehabilitation, <sup>3</sup>Department of Medicine and <sup>4</sup>Department of Biochemistry and Molecular Biology Mayo Clinic College of Medicine, Rochester, MN 55905, USA.

<sup>5</sup>Correspondence should be addressed to J.M.v.D. (e-mail: vandeursen.jan@mayo.edu)

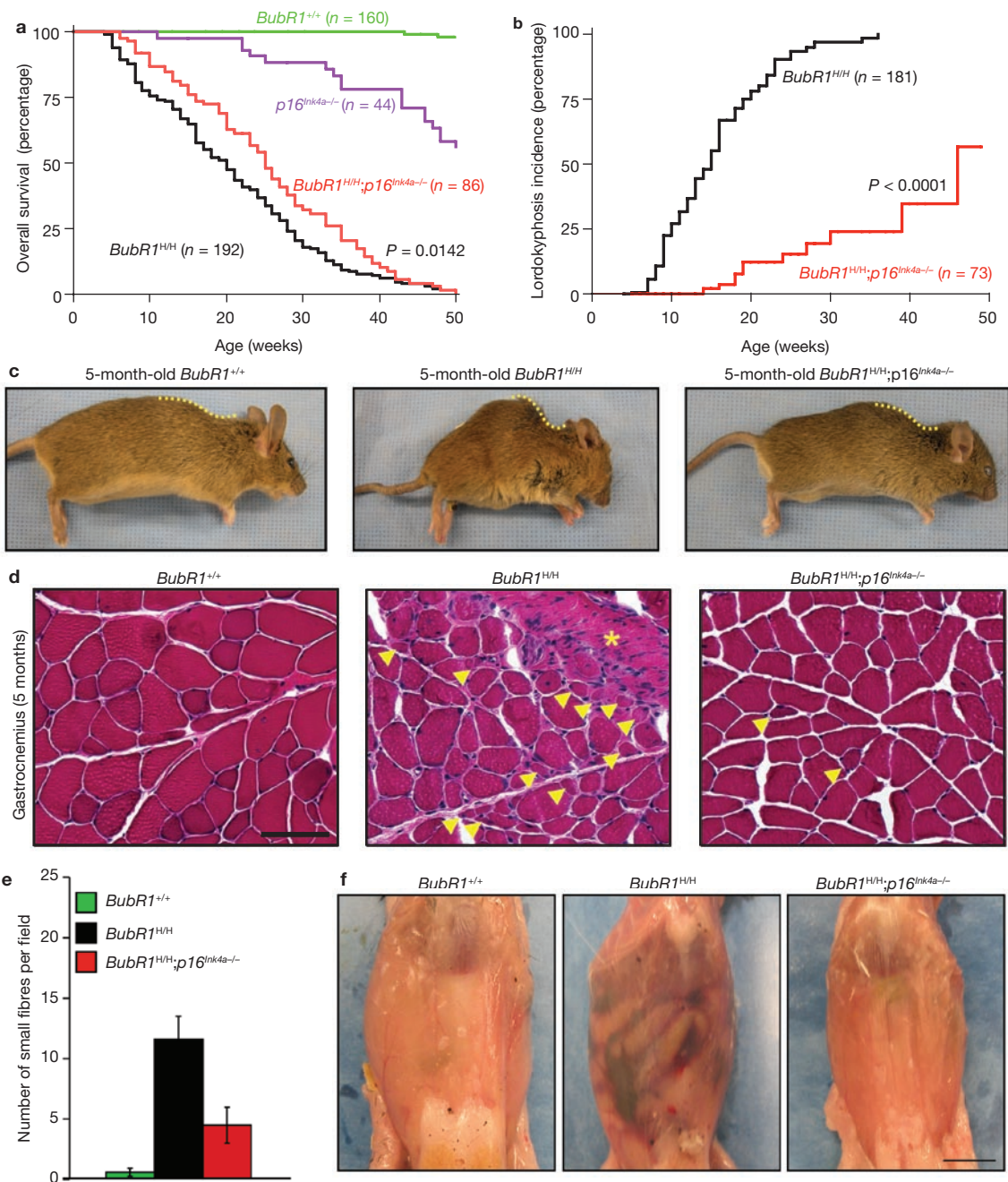


**Figure 1** Ablation of  $p16^{Ink4a}$  in  $BubR1^{H/H}$  mice extends lifespan and attenuates sarcopaenia. **(a)** Overall survival curves for wild-type,  $p16^{Ink4a-/-}$ ,  $BubR1^{H/H}$  and  $BubR1^{H/H};p16^{Ink4a-/-}$  mice. The median overall survival of combined  $BubR1^{H/H};p16^{Ink4a-/-}$  mice is 25 weeks, a 25% extension in lifespan compared with  $BubR1^{H/H}$  animals. We note that the  $p16^{Ink4a-/-}$ ,  $BubR1^{H/H}$  and  $BubR1^{H/H};p16^{Ink4a-/-}$  curves are all significantly different from the wild-type ( $BubR1^{+/+}$ ) curve ( $P < 0.0001$ , log-rank tests). Moreover, the  $BubR1^{H/H};p16^{Ink4a-/-}$  curve is significantly different from the  $BubR1^{H/H}$  curve ( $P = 0.0142$ ). **(b)** Incidence and latency of lordokyphosis in  $BubR1^{H/H}$  and  $BubR1^{H/H};p16^{Ink4a-/-}$  mice. The curves are significantly different ( $P < 0.0001$ , log-rank test). We note that no wild-type or  $p16^{Ink4a-/-}$  mice developed lordokyphosis during our one-year observation period (data not shown).

**$p16^{Ink4a}$  loss blunts sarcopaenia induced by BubR1 insufficiency**  
A prominent ageing-associated phenotype of  $BubR1^{H/H}$  mice is the development of lordokyphosis<sup>13</sup>. The incidence of this phenotype was

markedly reduced in  $BubR1^{H/H};p16^{Ink4a-/-}$  animals when compared with  $BubR1^{H/H}$  mice (Fig. 1b, c). Furthermore, the median time to onset of lordokyphosis was three times longer in  $BubR1^{H/H};p16^{Ink4a-/-}$  mice

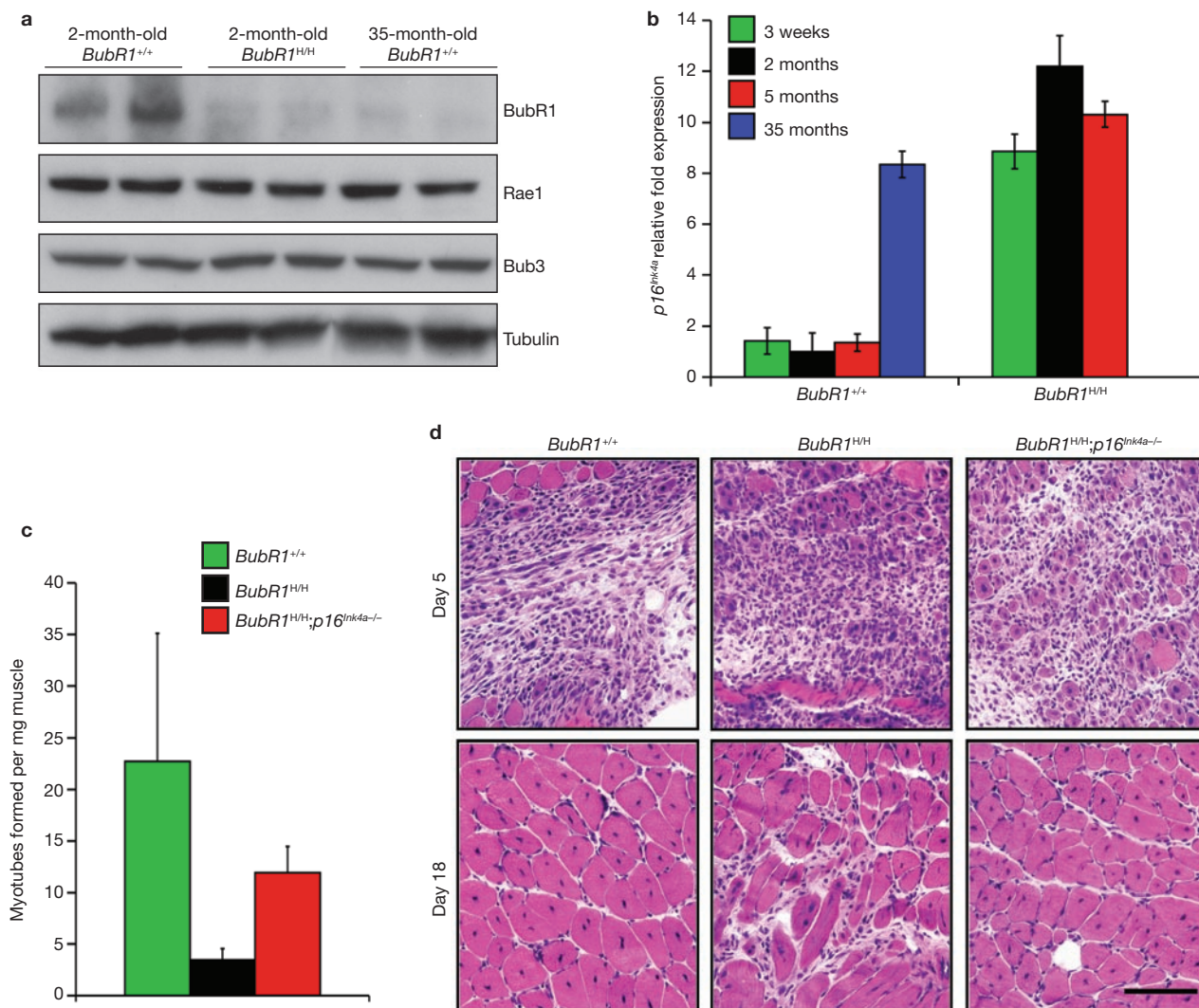


**Figure 2** Inverse correlation between BubR1 and p16<sup>Ink4a</sup> expression levels with ageing. **(a)** Western blot analysis of gastrocnemius muscle in young wild-type and *BubR1*<sup>H/H</sup> mice and old wild-type mice. Blots were probed with antibodies against BubR1, Bub3 and Rae1. Anti-tubulin was used as a loading control. Note that the mitotic checkpoint proteins Bub3 and Rae1 remain highly expressed as wild-type mice age. Uncropped images of the scans are shown in Supplementary Information, Fig. S6a. **(b)** p16<sup>Ink4a</sup> expression in wild-type and *BubR1*<sup>H/H</sup> gastrocnemius muscles at various ages analysed by qRT-PCR. Data are mean  $\pm$  s.d. ( $n = 3$  males per genotype and age group, with triplicate measurements taken). Values were normalized to *GAPDH*. Relative

fold expression is to 2-month-old wild-type values. **(c)** Myotube formation potential of gastrocnemius muscles from 5-month-old mice of the indicated genotypes analysed by a well-standardized *in vitro* assay. Data are mean  $\pm$  s.d. ( $n = 4$ ). **(d)** Cardiotoxin-treated gastrocnemius muscle of 5-month-old wild-type, *BubR1*<sup>H/H</sup> and *BubR1*<sup>H/H</sup>;p16<sup>Ink4a</sup><sup>-/-</sup> mice at 5 or 18 days after injection. Note that all gastrocnemius muscles show an extensive hypercellular response to cardiotoxin injection by day 5 regardless of genotype. Wild-type and *BubR1*<sup>H/H</sup>;p16<sup>Ink4a</sup><sup>-/-</sup> mice have complete restoration of muscle architecture by myofibers with central nuclei by day 18, whereas *BubR1*<sup>H/H</sup> mice have been unable to restore normal tissue structure. Scale bar is 100  $\mu$ m.

than in *BubR1*<sup>H/H</sup> mice (Fig. 1b). Lordokyphosis is associated with both osteoporosis and age-related degenerative loss of muscle mass and strength (sarcopaenia) in wild-type mice of extremely advanced age<sup>16</sup>. Histological evaluation of longitudinal femur sections from kyphotic *BubR1*<sup>H/H</sup> mice revealed no evidence for osteoporosis (Supplementary Information, Fig. S1a, b). Histopathology on gastrocnemius and paraspinal muscles of 5-month-old *BubR1*<sup>H/H</sup> mice, however, revealed clear signs of skeletal muscle atrophy and degeneration (Fig. 1d and data not shown). Muscle degeneration was greatly reduced in *BubR1*<sup>H/H</sup> muscles lacking p16<sup>Ink4a</sup> (Fig. 1d, e). In addition, abdominal muscles of *BubR1*<sup>H/H</sup> mice were poorly developed, as revealed by macroscopic analysis and magnetic resonance imaging (Fig. 1f; Supplementary Information, Fig. S1c). Depletion of p16<sup>Ink4a</sup> resulted in substantial

correction of this defect. These data demonstrate that p16<sup>Ink4a</sup> has a major role in establishing sarcopaenia in *BubR1*<sup>H/H</sup> mice.

p16<sup>Ink4a</sup> limits the regenerative capacity of  $\beta$  cells and has been linked to pancreatic islet atrophy and development of diabetes<sup>9,17,18</sup>, which in turn can cause muscle atrophy through accelerated degradation of muscle protein<sup>19</sup>. This prompted us to test whether the sarcopaenia observed in *BubR1*<sup>H/H</sup> mice might be due to  $\beta$  cell failure. *BubR1*<sup>H/H</sup> mice showed highly efficient glucose clearance in a glucose-tolerance test (Supplementary Information, Fig. S2a). Complementary blood insulin measurements indicated that insulin sensitivity was not impaired in *BubR1*<sup>H/H</sup> mice and showed no evidence for insulin resistance (Supplementary Information, Fig. S2b). Furthermore, overall pancreatic morphology, as well as islet size, shape and abundance were similar

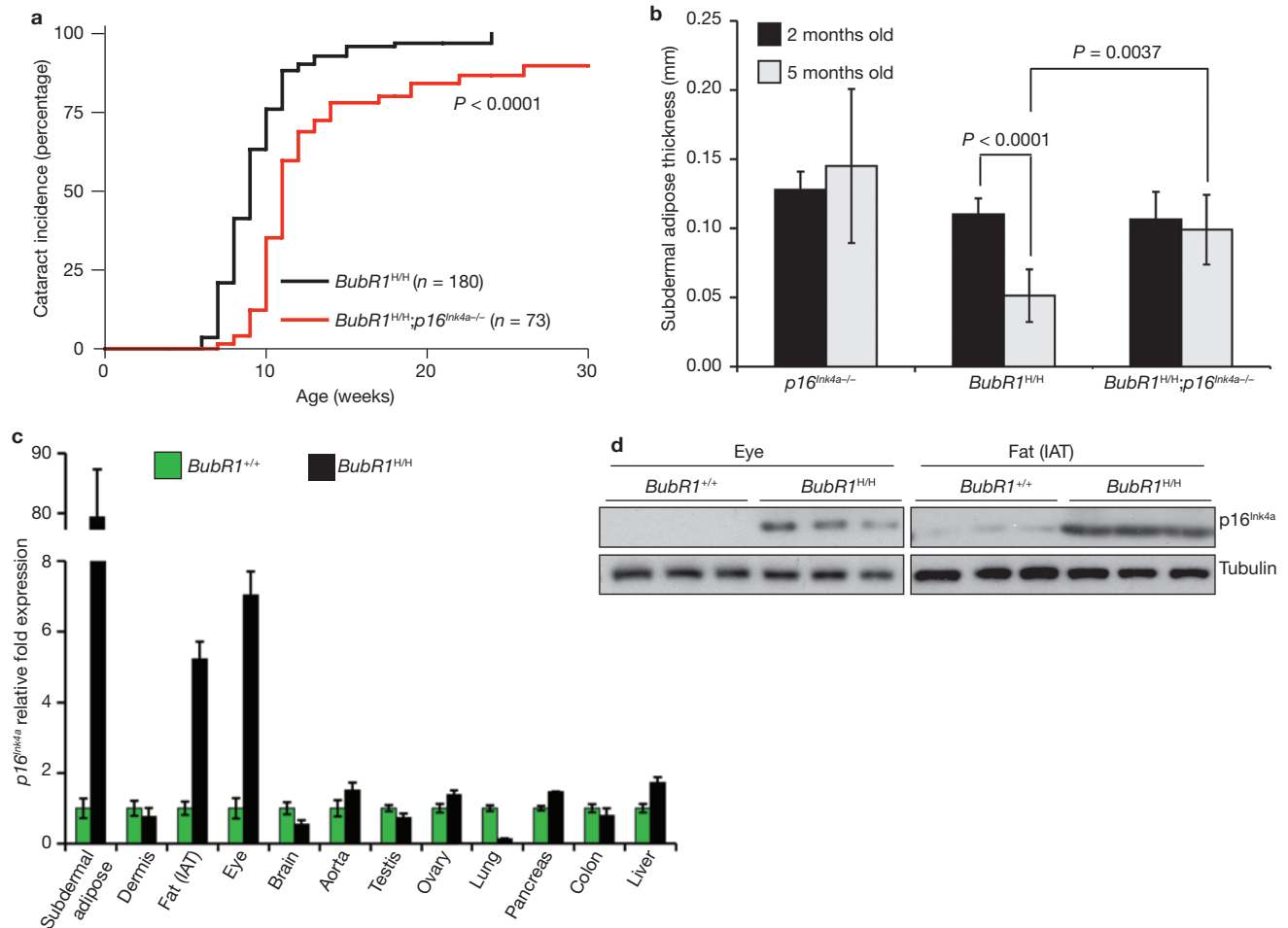


**Figure 3** *p16<sup>Ink4a</sup>* disruption attenuates selective progeroid features of *BubR1* hypomorphic mice. **(a)** Incidence and latency of cataract formation in *BubR1<sup>H/H</sup>* and *BubR1<sup>H/H</sup>;p16<sup>Ink4a</sup><sup>-/-</sup>* mice as detected by the use of slit light after dilation of eyes. The curves are significantly different ( $P < 0.0001$ , log-rank test). We note that no wild-type or *p16<sup>Ink4a</sup><sup>-/-</sup>* mice developed cataracts during this observation period. **(b)** Subcutaneous adipose layer thickness of *p16<sup>Ink4a</sup><sup>-/-</sup>*, *BubR1<sup>H/H</sup>* and *BubR1<sup>H/H</sup>;p16<sup>Ink4a</sup><sup>-/-</sup>* mice at 2 and 5 months of age. Data are mean  $\pm$  s.d. ( $n = 4$  male mice for each age per genotype). A two-tailed Mann-Whitney test

was used for statistical analysis. **(c)** qRT-PCR analysis for relative expression of *p16<sup>Ink4a</sup>* in a variety of 2-month-old tissues from *BubR1<sup>H/H</sup>* and wild-type mice. Values were normalized to *GAPDH*, and relative fold is to 2-month-old wild-type samples. Data are mean  $\pm$  s.d. ( $n = 3$  male mice for each tissue, with triplicate measurements taken). **(d)** Western blots of eye and fat extracts from 2-month-old *BubR1<sup>+/+</sup>* and *BubR1<sup>H/H</sup>* mice probed with anti-*p16<sup>Ink4a</sup>* antibody. Anti-tubulin antibody served as loading control. Uncropped images of the scans are shown in Supplementary Information, Fig. S6b, c.

in 12-month-old *BubR1<sup>H/H</sup>* and control mice, as verified by histology (Supplementary Information, Fig. S2c). Consistently, *p16<sup>Ink4a</sup>* expression in the pancreas was not significantly elevated in *BubR1<sup>H/H</sup>* mice, compared with *BubR1<sup>+/+</sup>* counterparts. Thus, sarcopaenia in *BubR1<sup>H/H</sup>* mice is unlikely to be caused by *p16<sup>Ink4a</sup>*-mediated  $\beta$  cell degeneration or insulin resistance.

### **BubR1 and *p16<sup>Ink4a</sup>* levels are inversely linked in skeletal muscle**

To determine whether *BubR1* may have a role in normal skeletal muscle ageing, we measured *BubR1* protein levels in skeletal muscle of young and old wild-type mice by western blot analysis. Gastrocnemius muscles had considerably higher levels of *BubR1* protein at 2 months than at 35 months of age (Fig. 2a; Supplementary Information, Fig. S6a). *BubR1* transcripts were undetectable by qRT-PCR in the gastrocnemius of 35-month-old mice but were readily present at 2 months (data not shown), suggesting that reduced *BubR1* transcriptional activity contributes to the decline in *BubR1* protein levels at advanced age. In contrast to *BubR1* transcription, *p16<sup>Ink4a</sup>* transcription increased markedly with age

in gastrocnemius muscles of old wild-type mice (Fig. 2b). Gastrocnemius of 2- and 5-month-old *BubR1<sup>H/H</sup>* mice also had high *p16<sup>Ink4a</sup>* transcript levels (Fig. 2b), providing evidence for an inverse relationship between *BubR1* and *p16<sup>Ink4a</sup>* expression. To characterize this relationship further, we measured *p16<sup>Ink4a</sup>* expression in gastrocnemius of 3-week-old *BubR1<sup>H/H</sup>* mice, when skeletal muscle atrophy is histologically undetectable (Supplementary Information, Fig. S2d). Transcript levels of *p16<sup>Ink4a</sup>* were similarly elevated for 3-week-old, and 2- and 5-month-old mice (Fig. 2b), indicating that *p16<sup>Ink4a</sup>* induction is an early response to *BubR1* hypomorphism that precedes histological signs of sarcopaenia.

Increased expression of *p16<sup>Ink4a</sup>* with age in adult stem cells is associated with reduced tissue repair and regeneration in several mouse tissues<sup>9–12</sup>. To explore whether *p16<sup>Ink4a</sup>*-mediated exhaustion of myogenic stem-cell potential might contribute to premature sarcopaenia in *BubR1<sup>H/H</sup>* mice, *in vitro* myoblast-to-myofibre differentiation assays were performed on gastrocnemius muscles from 5-month-old wild-type, *BubR1<sup>H/H</sup>* and *BubR1<sup>H/H</sup>;p16<sup>Ink4a</sup><sup>-/-</sup>* mice. In these assays, the average number of myotubes obtained per milligram of muscle tissue was about 7-fold lower in

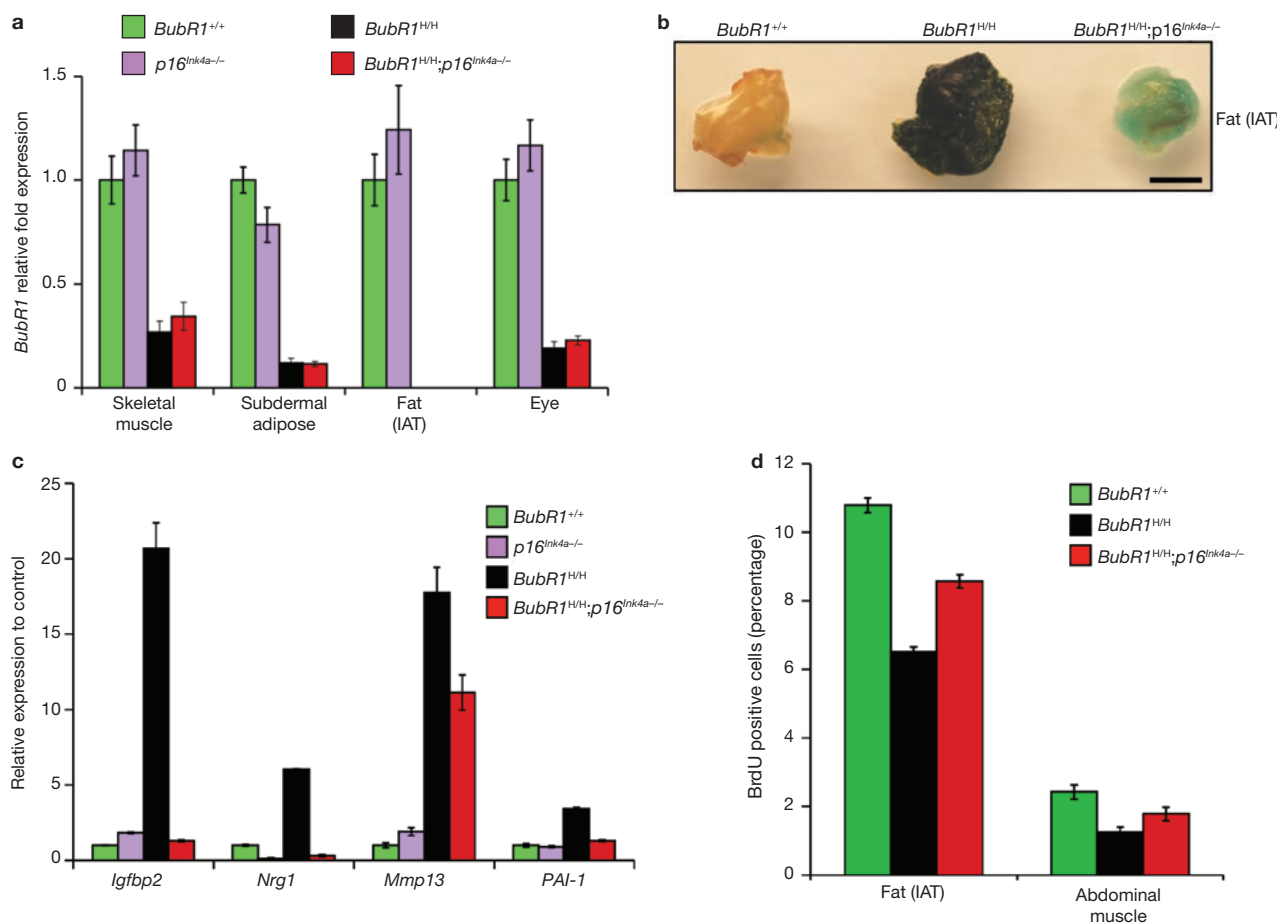


**Figure 4** *p16*<sup>Ink4a</sup> induction in *BubR1*<sup>H/H</sup> mice promotes cellular senescence.

(a) Relative expression of *BubR1* in gastrocnemius, subdermal adipose, fat deposits and eyes from 2-month-old wild-type, *p16*<sup>Ink4a-/-</sup>, *BubR1*<sup>H/H</sup> and *BubR1*<sup>H/H</sup>;*p16*<sup>Ink4a-/-</sup> mice as determined by qRT-PCR. Values were normalized to *GAPDH*. Relative fold is to 2-month-old wild-type samples. Data are mean  $\pm$  s.d. ( $n = 3$  male mice per genotype, with triplicate measurements taken per sample). We note that ablation of *p16*<sup>Ink4a</sup> was unable to increase the amount of *BubR1* present in either wild-type or *BubR1* hypomorphic mice. (b) IAT of 5-month-old wild-type, *BubR1*<sup>H/H</sup>

and *BubR1*<sup>H/H</sup>;*p16*<sup>Ink4a-/-</sup> mice stained for SA- $\beta$ -galactosidase activity. Scale bar is 2 mm. (c) Relative expression of senescence markers in gastrocnemius muscles of 2-month-old wild-type, *p16*<sup>Ink4a-/-</sup>, *BubR1*<sup>H/H</sup> and *BubR1*<sup>H/H</sup>;*p16*<sup>Ink4a-/-</sup> mice analysed by qRT-PCR. Data are mean  $\pm$  s.d. ( $n = 3$  male mice per genotype). Values were normalized to *GAPDH*. Relative fold expression is to 2-month-old wild-type muscle. (d) Analysis of replicative senescence in skeletal muscle and fat of 2-month-old wild-type, *BubR1*<sup>H/H</sup> and *BubR1*<sup>H/H</sup>;*p16*<sup>Ink4a-/-</sup> mice by analysing *in vivo* BrdU incorporation. Data are mean  $\pm$  s.d. ( $n = 3$  males per genotype).

*BubR1*<sup>H/H</sup> mice than in wild-type mice (Fig. 2c). By contrast, only a 2-fold reduction in myotube formation was observed in *BubR1*<sup>H/H</sup> mice lacking *p16*<sup>Ink4a</sup>. To confirm these data, 5-month-old wild-type, *BubR1*<sup>H/H</sup> and *BubR1*<sup>H/H</sup>;*p16*<sup>Ink4a-/-</sup> mice were challenged to regenerate muscle fibres by injection of cardiotoxin, a 60-amino-acid polypeptide that causes acute injury by rapidly destroying muscle fibres<sup>20</sup>. Consistent with our *in vitro* data, muscle regeneration was overtly delayed in *BubR1*<sup>H/H</sup> mice, but not in *BubR1*<sup>H/H</sup>;*p16*<sup>Ink4a-/-</sup> counterparts (Fig. 2d). Collectively, these data indicate that *p16*<sup>Ink4a</sup> promotes sarcopaenia in *BubR1*<sup>H/H</sup> mice, at least in part, by impairing muscle regeneration.

#### ***p16*<sup>Ink4a</sup> loss attenuates ageing in selective *BubR1* hypomorphic tissues**

Loss of *p16*<sup>Ink4a</sup> caused a modest, yet significant, delay in the latency of cataract formation in *BubR1*<sup>H/H</sup> mice (Fig. 3a). Aged skin is characterized by reduced dermal thickness and subcutaneous adipose tissue, both of which are observed in *BubR1*<sup>H/H</sup> mice at young ages<sup>13</sup>. At 2 months of age, *BubR1*<sup>H/H</sup>, *BubR1*<sup>H/H</sup>;*p16*<sup>Ink4a-/-</sup> and *p16*<sup>Ink4a-/-</sup> mice had similar amounts

of subdermal adipose tissue (Fig. 3b). As expected, the mean thickness of the subcutaneous adipose layer decreased notably in 5-month-old *BubR1*<sup>H/H</sup> mice. This decline was not accompanied by increased fat storage in liver tissue (Supplementary Information, Fig. S2e). The decrease in subcutaneous fat was much less severe in age-matched *BubR1*<sup>H/H</sup>;*p16*<sup>Ink4a-/-</sup> mice (Fig. 3b), indicating that *p16*<sup>Ink4a</sup> is, at least in part, responsible for loss of subcutaneous adipose tissue in *BubR1*<sup>H/H</sup> mice. Tolerance of anaesthetic stress was also greatly improved in *BubR1*<sup>H/H</sup>;*p16*<sup>Ink4a-/-</sup> mice (Supplementary Information, Table S1), as was adipose tissue deposition (Supplementary Information, Fig. S2f). However, several progeroid symptoms seen in *BubR1*<sup>H/H</sup> mice remained unchanged following loss of *p16*<sup>Ink4a</sup>, including dwarfism, dermal thinning, arterial wall stiffening and infertility (Supplementary Information, Table S1 and data not shown). No progeroid phenotypes of *BubR1*<sup>H/H</sup> mice were aggravated by *p16*<sup>Ink4a</sup> loss.

The differential corrective effects of *p16*<sup>Ink4a</sup> disruption on individual progeroid phenotypes suggest tissue-specific differences in engagement of the *p16*<sup>Ink4a</sup> pathway in the cellular response to *BubR1* deficiency. *BubR1*<sup>H/H</sup> tissues in which *p16*<sup>Ink4a</sup> loss causes a significant

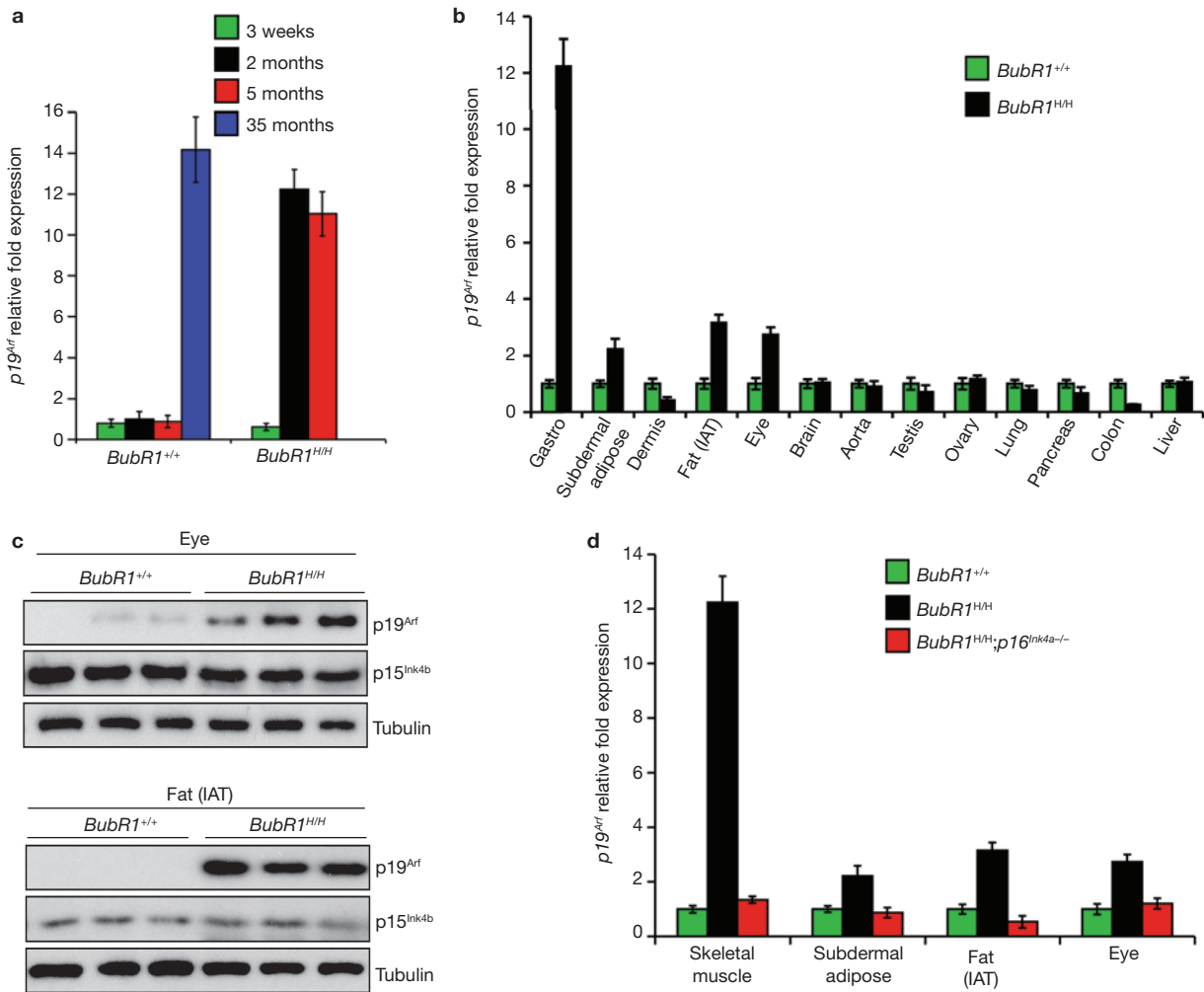


**Figure 5** *p19<sup>Arf</sup>* is elevated in *BubR1* hypomorphic tissues with high *p16<sup>Ink4a</sup>*. (a) Skeletal muscles of wild-type and *BubR1*<sup>HHH</sup> mice of various ages were analysed for *p19<sup>Arf</sup>* expression by qRT-PCR. All values were normalized to *GAPDH*. Data are mean  $\pm$  s.d. ( $n = 3$  mice were used per genotype and age group). (b) Relative expression of *p19<sup>Arf</sup>* in various tissues of 2-month-old *BubR1*<sup>HHH</sup> and *BubR1*<sup>+/+</sup> mice as measured by qRT-PCR. Data are mean  $\pm$  s.d. ( $n = 3$  males per genotype). All values were normalized to *GAPDH*. Relative expression is to wild-type samples. (c) Western blots of

eye and fat extracts from 2-month-old *BubR1*<sup>+/+</sup> and *BubR1*<sup>HHH</sup> mice probed with anti-*p19<sup>Arf</sup>* and *p15<sup>Ink4b</sup>* antibodies. Anti-tubulin antibody was used as a loading control. Uncropped images of the scans are shown in Supplementary Information, Fig. S6b, c. (d) Relative expression of *p19<sup>Arf</sup>* in skeletal muscle (gastrocnemius), subdermal adipose, fat deposits and eyes of 2-month-old wild-type, *BubR1*<sup>HHH</sup> and *BubR1*<sup>HHH</sup>; *p16<sup>Ink4a</sup>*<sup>-/-</sup> mice as determined by qRT-PCR. Data are mean  $\pm$  s.d. ( $n = 3$  males per genotype). All values were normalized to *GAPDH*. Relative expression is to wild-type samples.

delay of premature ageing, such as eye and (subdermal) adipose tissue, showed strong induction of *p16<sup>Ink4a</sup>* expression in response to *BubR1* hypomorphism (Fig. 3c, d; Supplementary Information, Fig. S6b, c). *BubR1*<sup>HHH</sup> tissues in which *p16<sup>Ink4a</sup>* inactivation has no discernible corrective effect, such as dermis, brain, aorta, testis and ovary, did not exhibit significant *p16<sup>Ink4a</sup>* induction (Fig. 3c and data not shown). Furthermore, mutant tissues that are not subjected to premature ageing, including lung, pancreas, colon and liver<sup>13</sup>, maintained low *p16<sup>Ink4a</sup>* expression levels. Together, these data demonstrate that *p16<sup>Ink4a</sup>* is activated in a subset of tissues in *BubR1*<sup>HHH</sup> mice, where it contributes to progeroid phenotypes.

#### *p16<sup>Ink4a</sup>* loss attenuates *in vivo* senescence

*BubR1* is a putative E2F-regulated gene<sup>21</sup> and loss of *p16<sup>Ink4a</sup>* leads to increased E2F transcriptional activity<sup>22</sup>. Accordingly, attenuation of ageing in skeletal muscle, fat and eye may be the result of increased *BubR1*

gene expression. However, this is unlikely as *BubR1* transcript levels in these tissues were not affected by loss of *p16<sup>Ink4a</sup>* (Fig. 4a). As *p16<sup>Ink4a</sup>* is an effector of cellular senescence, *p16<sup>Ink4a</sup>* deletion may delay ageing in hypomorphic mice by decreasing senescence. As shown in Fig. 4b, *BubR1*<sup>HHH</sup> adipose tissue expresses high levels of senescence-associated (SA)- $\beta$ -galactosidase, a marker of cellular senescence<sup>23</sup>. SA- $\beta$ -galactosidase staining was much lower in adipose tissue of *BubR1*<sup>HHH</sup>; *p16<sup>Ink4a</sup>*<sup>-/-</sup> mice (Fig. 4b). Skeletal muscles of 2-month-old *BubR1*<sup>HHH</sup> mice did not stain positive for SA- $\beta$ -galactosidase but expressed high levels of several other senescence-associated genes, including *Igf1*, *Nrg1*, *Mmp13* and *PAI-1*<sup>24-27</sup> (Fig. 4c). Expression of these markers was decreased markedly in skeletal muscles of age-matched *BubR1*<sup>HHH</sup>; *p16<sup>Ink4a</sup>*<sup>-/-</sup> mice. A key feature of senescence is loss of proliferative potential. *In vivo* 5-bromo-2-deoxyuridine (BrdU) labelling showed that 2-month-old *BubR1*<sup>HHH</sup> mice had much lower percentages of cycling cells in skeletal muscle and fat than wild-type mice (Fig. 4d). These reductions were less profound in

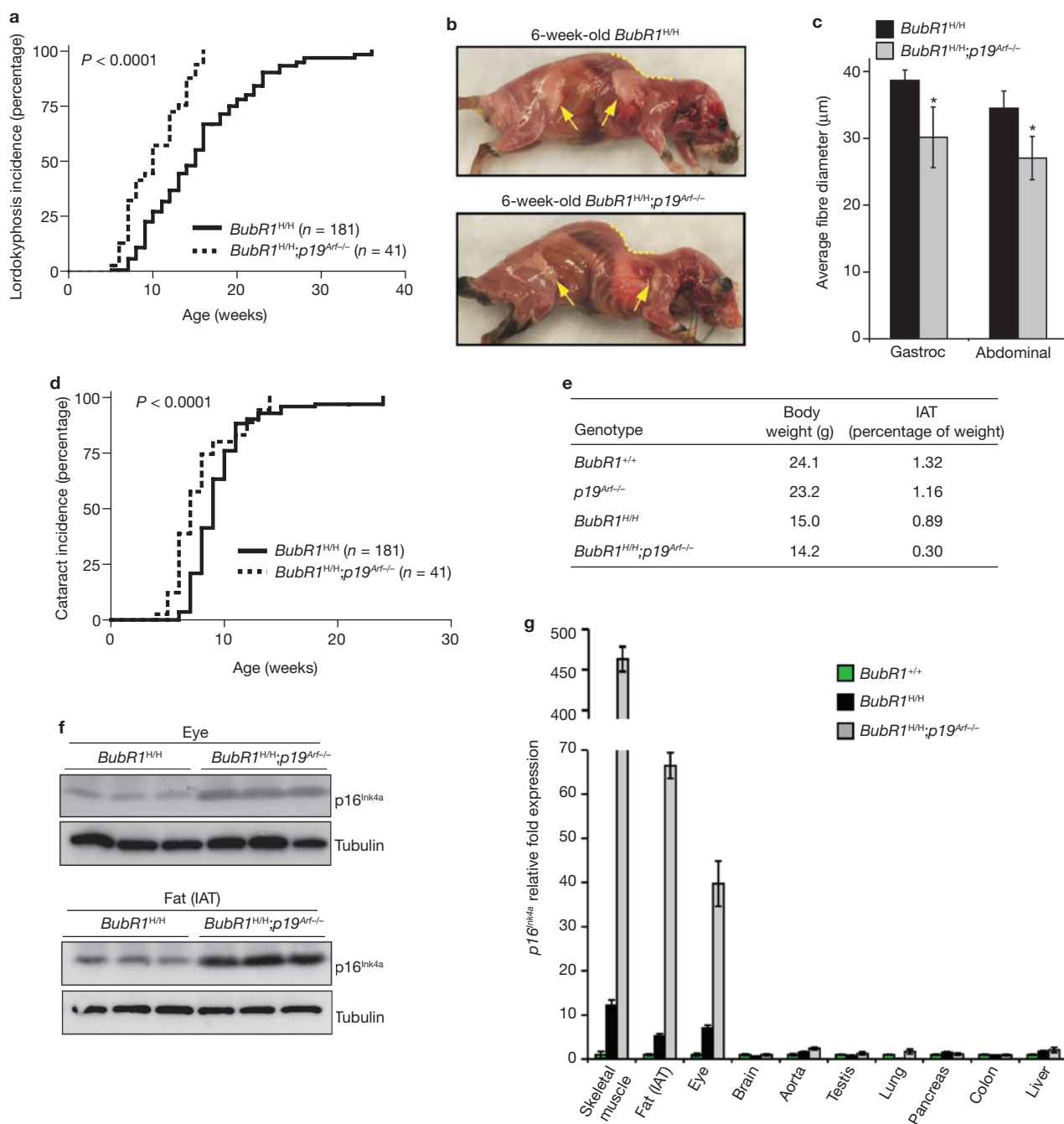


**Figure 6** Accelerated ageing in *BubR1*<sup>H/H</sup> mouse tissues with increased *p16*<sup>Ink4a</sup> expression when *p19*<sup>Arf</sup> is lacking. **(a)** Incidence and latency of lordokypnosis in *BubR1*<sup>H/H</sup> and *BubR1*<sup>H/H</sup>;*p19*<sup>Arf-/-</sup> mice. The curves are significantly different ( $P < 0.0001$ , log-rank test). **(b)** Skinned 6-week-old *BubR1*<sup>H/H</sup> and *BubR1*<sup>H/H</sup>;*p19*<sup>Arf-/-</sup> males. Note that the *BubR1*<sup>H/H</sup>;*p19*<sup>Arf-/-</sup> mouse has more profound lordokypnosis (dotted line) and reduced subcutaneous fat deposits (arrows). **(c)** Average muscle fibre size of gastrocnemius (Gastroc) and abdominal muscles of *BubR1*<sup>H/H</sup> and *BubR1*<sup>H/H</sup>;*p19*<sup>Arf-/-</sup> males. Data are mean  $\pm$  s.d. ( $n = 3$  mice per genotype). A two-tailed Mann-Whitney test was used for statistics. For both comparisons,  $P < 0.0001$ . **(d)** Incidence and latency of cataract formation in *BubR1*<sup>H/H</sup>

and *BubR1*<sup>H/H</sup>;*p19*<sup>Arf-/-</sup> mice. The curves are significantly different ( $P < 0.0001$ , log-rank test). **(e)** Amount of inguinal adipose tissue in 6-week-old mice of the indicated genotypes. IAT is expressed as percentage of total body weight. Three male mice of each genotype were used. **(f)** Western blots of eye and fat extracts from 2-month-old *BubR1*<sup>H/H</sup> and *BubR1*<sup>H/H</sup>;*p19*<sup>Arf-/-</sup> mice probed with anti-*p16*<sup>Ink4a</sup> and anti-tubulin antibody. Uncropped images of the scans are shown in Supplementary Information, Fig. S6d. **(g)** Relative expression of *p16*<sup>Ink4a</sup> in various tissues of 2-month-old *BubR1*<sup>+/+</sup>, *BubR1*<sup>H/H</sup> and *BubR1*<sup>H/H</sup>;*p19*<sup>Arf-/-</sup> mice as measured by qRT-PCR. Data are mean  $\pm$  s.d. ( $n = 3$  males per genotype). All values were normalized to *GAPDH*. Relative expression is to wild-type samples.

*BubR1*<sup>H/H</sup>;*p16*<sup>Ink4a-/-</sup> mice. Collectively, these data suggest that BubR1 hypomorphism causes cellular senescence in adipose tissue and skeletal muscle through a *p16*<sup>Ink4a</sup>-dependent mechanism. As *p16*<sup>Ink4a</sup> inactivation

attenuates both senescence and ageing in these tissues, the mechanism by which BubR1 hypomorphism accelerates the ageing phenotypes may involve *p16*<sup>Ink4a</sup>-induced senescence.

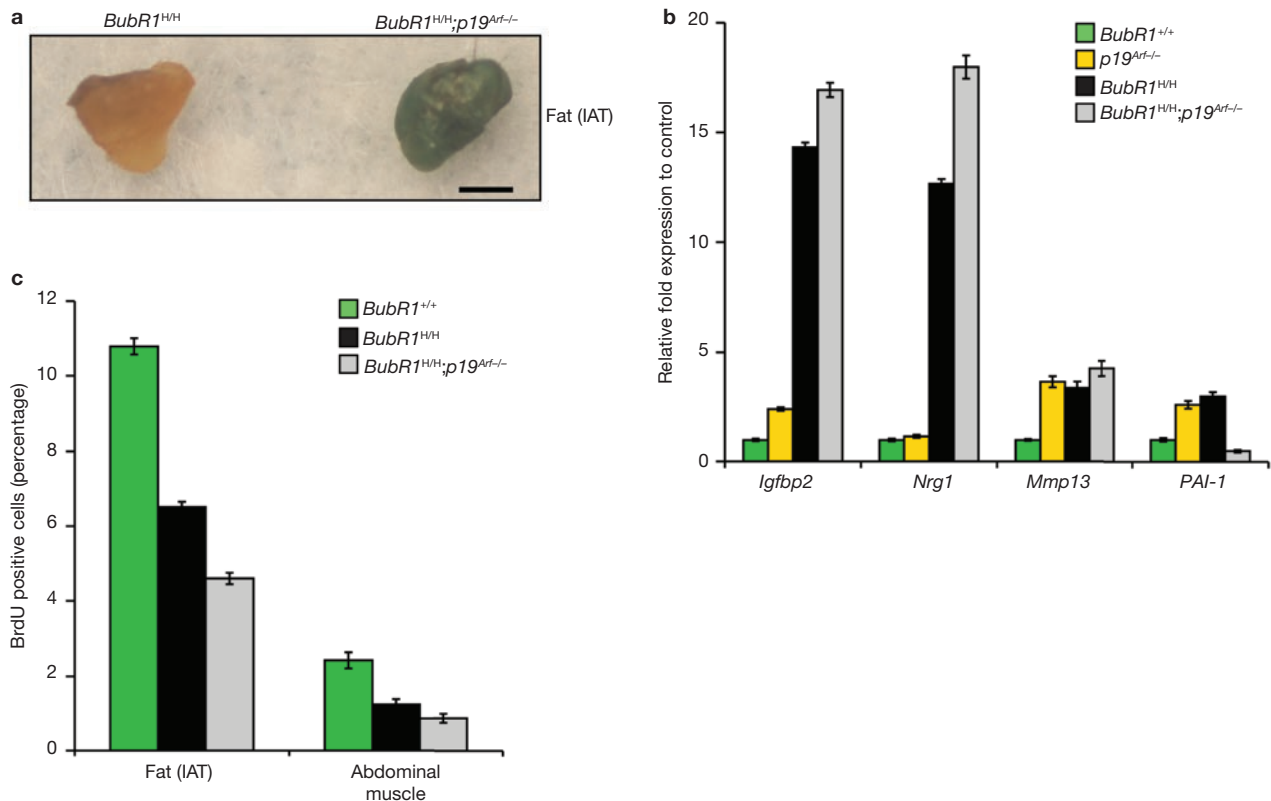


**Figure 7** Senescence increases in *BubR1*<sup>H/H</sup> tissues with high p16<sup>Ink4a</sup> when p19<sup>Arf</sup> is lacking. (a) IAT of 2-month-old *BubR1*<sup>H/H</sup> and *BubR1*<sup>H/H</sup>;*p19*<sup>Arf/-</sup> mice stained for SA-β-galactosidase activity. Scale bar is 2 mm. (b) Relative expression of senescence markers in gastrocnemius muscles of 6-week-old wild-type, *p19*<sup>Arf/-</sup>, *BubR1*<sup>H/H</sup> and *BubR1*<sup>H/H</sup>;*p19*<sup>Arf/-</sup> mice. All values were normalized

to *GAPDH*. Relative fold expression is to wild-type gastrocnemius. Data are mean ± s.d. (*n* = 3 male mice were evaluated per genotype). (c) Replicative senescence in skeletal muscle and fat of 2-month-old wild-type, *BubR1*<sup>H/H</sup> and *BubR1*<sup>H/H</sup>;*p19*<sup>Arf/-</sup> mice as analysed by *in vivo* BrdU incorporation. Data are mean ± s.d. (*n* = 3 male mice per genotype were used for this experiment).

### p19<sup>Arf</sup> is elevated in *BubR1*<sup>H/H</sup> tissues with high levels of p16<sup>Ink4a</sup>

Besides p16<sup>Ink4a</sup>, p19<sup>Arf</sup> is expressed at increased levels in many tissues of wild-type mice with advanced age<sup>7</sup>, including skeletal muscle (Fig. 5a). Although p19<sup>Arf</sup> is an established effector of senescence in cultured mouse embryonic fibroblasts (MEFs), its role in senescence and ageing in the context of the whole organism has not been clarified<sup>1,2</sup>. To explore the role of p19<sup>Arf</sup> in BubR1-mediated ageing, we analysed its relative expression in tissues from 2-month-old *BubR1*<sup>H/H</sup> and *BubR1*<sup>+/+</sup> mice. Increased p19<sup>Arf</sup> expression was consistently observed in *BubR1*<sup>H/H</sup> tissues that were subjected to premature ageing and had high p16<sup>Ink4a</sup> levels, including skeletal muscle, (subdermal) adipose tissue and eye, but not in tissues that developed age-related pathology in a p16<sup>Ink4a</sup>-independent fashion or had no age-related phenotypes (Fig. 5b, c; Supplementary Information, Fig. S6b, c and data not shown). Skeletal muscle, (subdermal) adipose tissue and eye from *BubR1*<sup>H/H</sup> mice lacking p16<sup>Ink4a</sup> had normal p19<sup>Arf</sup> transcript levels (Fig. 5d), suggesting that the observed increase in p19<sup>Arf</sup> expression is dependent on high p16<sup>Ink4a</sup> levels. p15<sup>Ink4b</sup>, which encodes a Cdk inhibitor that has been linked to ageing in some tissues<sup>7</sup>, was neither increased in *BubR1*<sup>H/H</sup> tissues with increased p16<sup>Ink4a</sup> and p19<sup>Arf</sup> expression, nor in any other tissue of *BubR1*<sup>H/H</sup> mice (Supplementary Information, Figs S3a, S6b, c). In contrast to p16<sup>Ink4a</sup> and p19<sup>Arf</sup>, p15<sup>Ink4b</sup> was not expressed at increased levels in skeletal muscles of aged wild-type mice (Supplementary Information, Fig. S3b).

### p19<sup>Arf</sup> disruption accelerates ageing in *BubR1*<sup>H/H</sup> mice

To determine whether p19<sup>Arf</sup> also acts as an effector of ageing in *BubR1*<sup>H/H</sup> mice, 41 *BubR1*<sup>H/H</sup>;*p19*<sup>Arf/-</sup> mice were generated and monitored for development of age-related phenotypes. Surprisingly, lordokyphosis developed at a significantly faster rate in *BubR1*<sup>H/H</sup>;*p19*<sup>Arf/-</sup> mice than in *BubR1*<sup>H/H</sup> mice (Fig. 6a, b). Six-week-old *BubR1*<sup>H/H</sup>;*p19*<sup>Arf/-</sup> mice had significantly smaller fibres in gastrocnemius and abdominal muscles than age-matched *BubR1*<sup>H/H</sup> mice (Fig. 6c; Supplementary Information, Fig. S4a), indicating that muscle wasting was accelerated in the absence of p19<sup>Arf</sup>. Cataract formation was also significantly accelerated when p19<sup>Arf</sup> was absent (Fig. 6d). Skinned 6-week-old *BubR1*<sup>H/H</sup>;*p19*<sup>Arf/-</sup> mice showed overt reductions in deposition of adipose tissue (Fig. 6b). This was confirmed by weighing inguinal adipose tissue (IAT, Fig. 6e). Furthermore, the mean thickness of the subcutaneous adipose layer was significantly smaller in *BubR1*<sup>H/H</sup>;*p19*<sup>Arf/-</sup> mice than in *BubR1*<sup>H/H</sup> mice (0.07 versus 0.11 mm; *P* < 0.0001, two-tailed Mann-Whitney test). Other progeroid features of *BubR1*<sup>H/H</sup> mice seemed to be unchanged by p19<sup>Arf</sup> inactivation (Supplementary Information, Fig. S4b and Table S1). Taken together, these data indicate that p19<sup>Arf</sup> acts to delay ageing in response to BubR1 hypomorphism.

One possible explanation for the pro-ageing effect of p19<sup>Arf</sup> inactivation in *BubR1*<sup>H/H</sup> mice may involve increased expression of p16<sup>Ink4a</sup>. Consistent with this idea, p16<sup>Ink4a</sup> levels in skeletal muscle, fat and eye increased markedly when p19<sup>Arf</sup> was knocked out in *BubR1*<sup>H/H</sup> mice (Fig. 6f, g; Supplementary Information, Fig. S6d). A potential

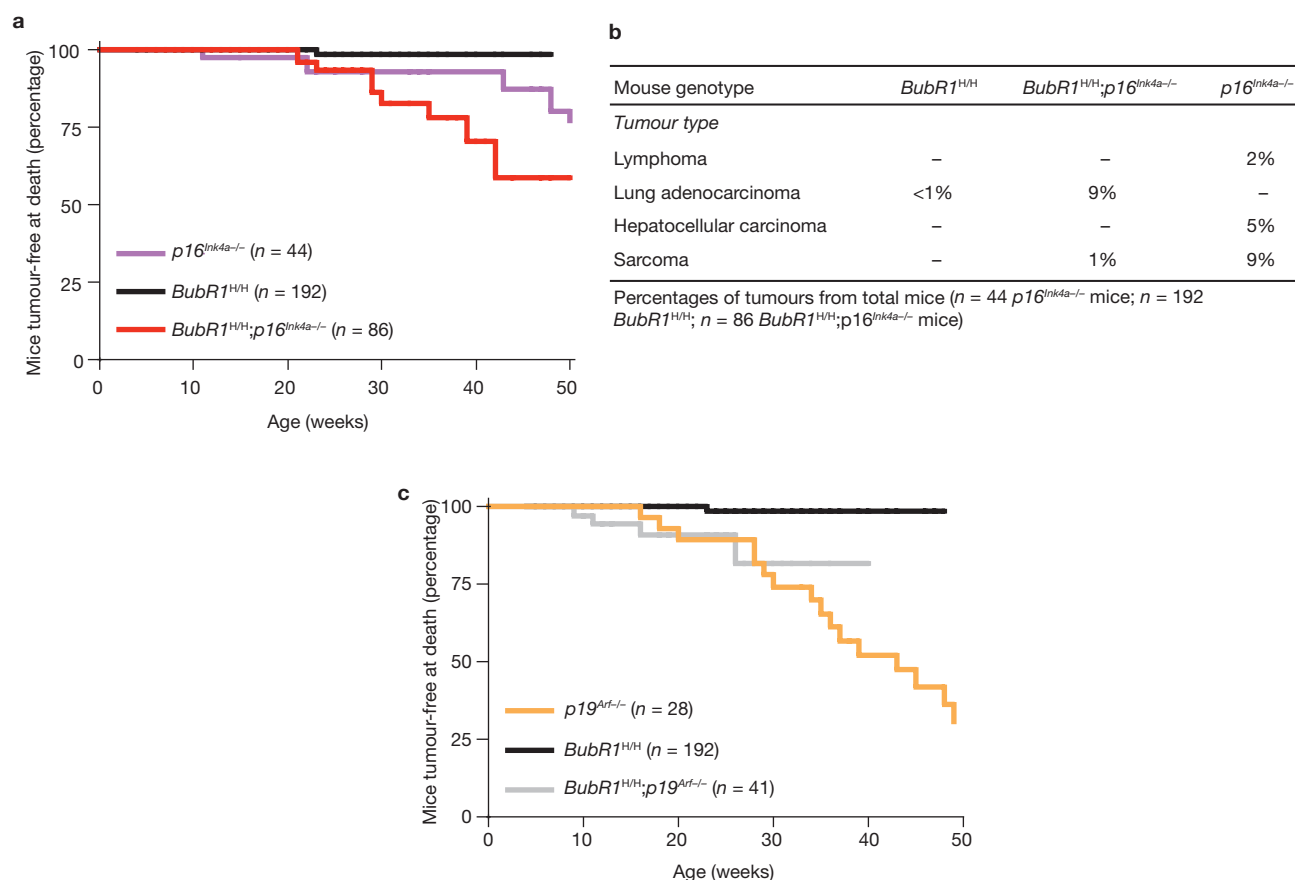


**Figure 8** Ablation of *p16*<sup>Ink4a</sup> accelerates lung tumorigenesis in *BubR1* insufficient mice. **(a)** Percentage of mice with tumours at time of death as a function of time for *p16*<sup>Ink4a-/-</sup>, *BubR1*<sup>H/H</sup> and *BubR1*<sup>H/H</sup>;*p16*<sup>Ink4a-/-</sup> mice. Biopsies were performed on moribund animals and all tissues were screened for tumours. Tumour tissues were collected and processed for histological confirmation. The *BubR1*<sup>H/H</sup>;*p16*<sup>Ink4a-/-</sup> curve

is significantly different from the *BubR1*<sup>H/H</sup> curve with  $P = 0.0027$  (calculated using a log-rank test). **(b)** Tumour spectra of *p16*<sup>Ink4a-/-</sup>, *BubR1*<sup>H/H</sup> and *BubR1*<sup>H/H</sup>;*p16*<sup>Ink4a-/-</sup> mice. **(c)** As in **a** but for *p19*<sup>Arf-/-</sup>, *BubR1*<sup>H/H</sup> and *BubR1*<sup>H/H</sup>;*p19*<sup>Arf-/-</sup> mice. There is no significant difference between the curves of *BubR1*<sup>H/H</sup>;*p19*<sup>Arf-/-</sup> and *p19*<sup>Arf-/-</sup> mice using a log-rank test.

explanation for these results may be that genetic manipulation of *p19*<sup>Arf</sup> sequences changes the normal regulatory balance in the *Cdkn2* locus, thereby increasing *p16*<sup>Ink4a</sup> expression. However, disruption of *p19*<sup>Arf</sup> had no appreciable effect on *p16*<sup>Ink4a</sup> levels in tissues undergoing *p16*<sup>Ink4a</sup>-independent ageing or lacking age-related pathologies (Fig. 6g), arguing against this possibility.

#### Inactivation of *p19*<sup>Arf</sup> increases cellular senescence

Next, we investigated whether *p19*<sup>Arf</sup> loss accelerates ageing in *BubR1*<sup>H/H</sup> mice through increased senescence. Indeed adipose tissue of 6-week-old *BubR1*<sup>H/H</sup>;*p19*<sup>Arf-/-</sup> mice showed much higher SA- $\beta$ -galactosidase activity than that of corresponding *BubR1*<sup>H/H</sup> mice (Fig. 7a). Furthermore, two senescence-associated genes, *Igf1p2* and *Nrg1*, which are expressed at increased levels in gastrocnemius muscles of 6-week-old *BubR1*<sup>H/H</sup> mice, were further elevated in corresponding muscles of age-matched *BubR1*<sup>H/H</sup>;*p19*<sup>Arf-/-</sup> mice (Fig. 7b). *In vivo* BrdU incorporation showed that cell proliferation in skeletal muscle and fat was considerably lower in *BubR1*<sup>H/H</sup>;*p19*<sup>Arf-/-</sup> mice than in *BubR1*<sup>H/H</sup> mice (Fig. 7c). Collectively, these data indicate that *p19*<sup>Arf</sup> induction in *BubR1*<sup>H/H</sup> mice functions to prevent or delay senescence and provide further evidence for the notion that *in vivo* senescence promotes ageing.

#### Distinct *in vivo* and *in vitro* effects of *p16*<sup>Ink4a</sup> and *p19*<sup>Arf</sup> inactivation on senescence

Previously, we have shown that *BubR1*<sup>H/H</sup> MEFs express high levels of *p16*<sup>Ink4a</sup> and *p19*<sup>Arf</sup> and age prematurely<sup>13</sup>. To determine the effects *p16*<sup>Ink4a</sup> and *p19*<sup>Arf</sup> on cellular senescence in these MEFs, we stained *BubR1*<sup>H/H</sup>;*p16*<sup>Ink4a-/-</sup> and *BubR1*<sup>H/H</sup>;*p19*<sup>Arf-/-</sup> MEFs for SA- $\beta$ -galactosidase. Inactivation of *p19*<sup>Arf</sup> caused a marked decrease in senescence in *BubR1*<sup>H/H</sup> MEFs, whereas inactivation of *p16*<sup>Ink4a</sup> had no effect (Supplementary Information, Fig. S5a, b). Consistently, the percentage of cycling cells was greatly increased in *BubR1*<sup>H/H</sup>;*p19*<sup>Arf-/-</sup> MEFs, but not in *BubR1*<sup>H/H</sup>;*p16*<sup>Ink4a-/-</sup> MEFs (Supplementary Information, Fig. S5c, d). Furthermore, *BubR1*<sup>H/H</sup>;*p19*<sup>Arf-/-</sup> MEFs grew considerably faster than *BubR1*<sup>H/H</sup> MEFs, but *BubR1*<sup>H/H</sup>;*p16*<sup>Ink4a-/-</sup> MEFs did not (Supplementary Information, Fig. S5e, f). Immunoblotting showed that the *p19*<sup>Arf</sup>-53 pathway remained highly active in *BubR1*<sup>H/H</sup>;*p16*<sup>Ink4a-/-</sup> MEFs, similarly to *BubR1*<sup>H/H</sup> MEFs, whereas it was inactive in *BubR1*<sup>H/H</sup>;*p19*<sup>Arf-/-</sup> MEFs (Supplementary Information, Fig. S5h, g). Together, these data demonstrate that the effects of *p16*<sup>Ink4a</sup> and *p19*<sup>Arf</sup> ablation on *in vivo* senescence in skeletal muscle and fat of *BubR1*<sup>H/H</sup> mice are not recapitulated by their effects on *in vitro* senescence in *BubR1*<sup>H/H</sup> MEFs.

## p16<sup>Ink4a</sup> loss synergizes with BubR1 insufficiency in lung tumorigenesis

*BubR1*<sup>H/H</sup> mice show progressive and severe aneuploidy but rarely develop tumours<sup>13</sup>. Activation of p16<sup>Ink4a</sup> or p19<sup>Arf</sup> in response to BubR1 hypomorphism may act to suppress tumorigenesis. To test for this possibility, *BubR1*<sup>H/H</sup> mice lacking p16<sup>Ink4a</sup> or p19<sup>Arf</sup> were monitored for tumour formation. Live *BubR1*<sup>H/H</sup>;p16<sup>Ink4a</sup><sup>-/-</sup> and *BubR1*<sup>H/H</sup> mice showed no overt tumours, but biopsy of moribund or dead animals revealed that *BubR1*<sup>H/H</sup>;p16<sup>Ink4a</sup><sup>-/-</sup> mice had significantly more tumours than *BubR1*<sup>H/H</sup> mice (Fig. 8a). Eight out of nine *BubR1*<sup>H/H</sup>;p16<sup>Ink4a</sup><sup>-/-</sup> tumours were lung adenocarcinomas, a type of tumour observed in only one *BubR1*<sup>H/H</sup> mouse and none of the p16<sup>Ink4a</sup><sup>-/-</sup> mice (Fig. 8b). Sarcomas, the most prevalent tumour type in p16<sup>Ink4a</sup><sup>-/-</sup> mice, were rare in *BubR1*<sup>H/H</sup>;p16<sup>Ink4a</sup><sup>-/-</sup> mice and not present in *BubR1*<sup>H/H</sup> mice. Thus, the effect of BubR1 insufficiency is synergistic with that of p16<sup>Ink4a</sup> loss during tumorigenesis in lung epithelial cells, but not in other cell types (see Supplementary Discussion). *BubR1*<sup>H/H</sup>;p19<sup>Arf</sup><sup>-/-</sup> and p19<sup>Arf</sup><sup>-/-</sup> mice, however, had overlapping tumour-free survival curves (Fig. 8c), indicating that BubR1 insufficiency and p19<sup>Arf</sup> loss do not synergize in tumorigenesis.

## DISCUSSION

Here, we report that inactivation of p16<sup>Ink4a</sup> attenuates the development of age-related pathologies in *BubR1*<sup>H/H</sup> tissues with elevated p16<sup>Ink4a</sup>. This shows that induction of p16<sup>Ink4a</sup> by cellular stress resulting from BubR1-insufficiency drives the development of ageing-associated phenotypes, and provides direct evidence for a causal involvement of this tumour suppressor in organismal ageing. Importantly, skeletal muscle and fat, two tissues that are subject to p16<sup>Ink4a</sup>-dependent ageing when BubR1 levels are low, have higher numbers of replicating cells and show decreased expression of senescence-associated proteins in the absence of p16<sup>Ink4a</sup>. These observations support the notion that p16<sup>Ink4a</sup> contributes to ageing-associated pathologies through accumulation of senescent cells. This is a significant finding as evidence that cellular senescence promotes ageing has thus far been largely circumstantial<sup>2,6</sup>.

*BubR1*<sup>H/H</sup> mouse tissues, in which p16<sup>Ink4a</sup> is elevated, also have increased p19<sup>Arf</sup>. However, p19<sup>Arf</sup> inactivation accelerates rather than delays ageing in these tissues, indicating that this tumour suppressor provides anti-ageing activity. This seems surprising, considering that p19<sup>Arf</sup> is an effector of senescence in cultured cells<sup>2,6</sup>. However, the recent observation that transgenic mice carrying an extra copy of both p19<sup>Arf</sup> and p53 are protected from ageing-associated damage and live longer than normal mice<sup>28</sup>, is consistent with our finding that p19<sup>Arf</sup> has anti-ageing activity in *BubR1*<sup>H/H</sup> mice. It has been proposed that the p19<sup>Arf</sup>-p53 pathway in response to low, chronic stress, may primarily induce genes that promote cell survival and repair, thereby extending lifespan<sup>5,28,29</sup>. High, acute types of stress, on the other hand, may accelerate ageing by triggering a more robust p53 response, causing irreversible cell-cycle arrest and/or apoptosis<sup>5,29-31</sup>. Therefore, one possibility is that p19<sup>Arf</sup> may elicit a p53 transcriptional response that provides protection against cellular stress resulting from BubR1 hypomorphism, thus delaying the onset of cellular senescence. The observation that skeletal muscle and fat from *BubR1*<sup>H/H</sup> mice lacking p19<sup>Arf</sup> accumulate more senescent cells is consistent with this idea. Strong additional support for the conclusion that p19<sup>Arf</sup> has anti-ageing activity is provided by our unpublished observations indicating that *BubR1*<sup>H/H</sup> mice lacking p53 phenocopy those lacking p19<sup>Arf</sup>. Two observations reported here suggest that p19<sup>Arf</sup> may

exert its anti-ageing effect, at least in part, through negative regulation of p16<sup>Ink4a</sup> expression. First, inactivation of p19<sup>Arf</sup> in *BubR1*<sup>H/H</sup> mice resulted in increased p16<sup>Ink4a</sup> expression in skeletal muscle, fat and eye, three tissues that have high p19<sup>Arf</sup> levels and are subjected to accelerated ageing. Second, inactivation of p16<sup>Ink4a</sup> prevented the induction of p19<sup>Arf</sup> in these *BubR1*<sup>H/H</sup> tissues. How p19<sup>Arf</sup> attenuates p16<sup>Ink4a</sup> expression remains to be addressed.

Although inactivation of p16<sup>Ink4a</sup> significantly delays the development of certain ageing-associated phenotypes in *BubR1*<sup>H/H</sup> mice, it does not completely prevent them. Furthermore, other progeroid phenotypes are not affected by loss of p16<sup>Ink4a</sup>. These findings suggest that BubR1 hypomorphism engages other progeroid effectors in addition to p16<sup>Ink4a</sup>. The identity of these effectors is currently unclear and remains to be established. Striking similarities exist between the progeroid phenotypes of *Bmal1* knockout and *BubR1*<sup>H/H</sup> mice<sup>32</sup>. The molecular basis of this similarity is unclear, although, based on the known roles of each protein, it is unlikely that BubR1 and *Bmal1* are functionally connected. However, it is possible that downstream pathways that respond to stress resulting from *Bmal1* loss and BubR1 hypomorphism are shared. □

## METHODS

**Generation of compound mutant mice.** *BubR1*<sup>H/H</sup> mice were generated as described previously<sup>13</sup>. p16<sup>Ink4a</sup> and p19<sup>Arf</sup> knockout mice have been generated previously and were acquired from the Mouse Models of Human Cancers Consortium located at the National Cancer Institute, Frederick<sup>33,34</sup>. All mice were on a mixed 129 × C57BL/6 genetic background. They were housed in a pathogen-free barrier environment for the duration of the study. Experimental procedures involving the use of these laboratory mice were reviewed and approved by the Institutional Animal Care and Use Committee of the Mayo Clinic. Prism software (GraphPad Software) was used for generation of all survival curves and for statistical analyses.

**Collection and analysis of tumours.** Moribund mice were killed and all major organs were screened for overt tumours using a dissection microscope. Tumours that were collected were processed by standard procedures for histopathology. A Fisher's exact test was used to compare tumour incidence proportions across the genotypes for mice that developed tumours. Board-certified pathologists assisted in the histological evaluation of tumour sections.

**Analysis of progeroid phenotypes.** Bi-weekly, mice were screened for the development of overt cataracts by examining dilated eyes with a slit-light. Incidence of lordokyphosis was checked bi-weekly. Mice that showed lordokyphosis for three consecutive monitoring periods were determined to have this condition. Various skeletal muscles were collected and processed for histology as described previously<sup>35,36</sup>. Fibre diameter measurements were performed on cross sections of gastrocnemius and abdominal muscles from 6-week-old male mice (*n* = 3 mice per genotype). A total of 50 fibres were measured per muscle using a calibrated computer program (Olympus MicroSuite Five). Dissection, histology and measurements of dermal and adipose layers of dorsal skin were performed as described previously<sup>16</sup>. Values represent an average of four males. Analysis of arterial wall stiffening was performed as described previously<sup>14</sup>. Measurements of body weight and IAT were performed on 6-week-old males (*n* = 3 per genotype). Oral glucose tolerance tests were performed on 5-month-old male mice (*n* = 5 per genotype) as described by the Jackson Laboratory (www.jax.org). Insulin measurements were performed as described previously<sup>37</sup>.

**Quantitative real-time PCR.** Total RNA was extracted from tissues using a Qiagen RNeasy RNA isolation kit according to the manufacturer's protocol. Transcription into cDNA was performed using random hexamers and SuperScript III reverse transcriptase (Invitrogen) according to the manufacturer's instructions. All PCR reactions used SYBR green PCR Master Mix (Applied Biosystems) to a final volume of 12 µl, with each cDNA sample performed in triplicate in the ABI PRISM 7900 Sequence Detection System (Applied Biosystems) according to the protocol of the manufacturer. All experiments were performed on organs/tissues from at least

three different animals in each age group and genotype. The expression of genes was normalized to *GAPDH*. Sequences of primers used for qRT-PCR of *p15<sup>Ink4b</sup>* (ref. 38), *p16<sup>Ink4a</sup>* (ref. 39), *p19<sup>Arf</sup>* (ref. 28), *BubR1* (ref. 40), *Mmp-13* (ref. 41), *PAI-1* (ref. 42), *Igfbp-2* (ref. 43), and *GAPDH* (ref. 44) were as published. Additionally, sequences for *Nrg1* were: forward, CATGGTGAACATAGCGAATGGCC; reverse, CCACAATATGCTCACTGGAGATG A. Statistical differences were determined using an unpaired two-tailed *t* test.

**Analysis of satellite-cell function.** Analysis of *in vivo* satellite-cell function were carried out as described previously<sup>20</sup>. Briefly, mice anaesthetized with avertin (200 mg kg<sup>-1</sup>, i.p.) were given a single 50- $\mu$ l injection of cardiotoxin (10  $\mu$ M; Calbiochem) into the gastrocnemius muscle. After this injection, the skin incision was closed with a nylon suture. Mice were allowed to recover and then were analysed at both 5 and 18 days post-injection by routine histology. Isolation and culture of skeletal muscle satellite cells were performed as described previously<sup>45</sup>. Briefly, hindlimb muscles of 5-month-old mice were removed and trimmed of excess connective tissue and fat. Minced muscles were subjected to several 15-min rounds of digestion at 37 °C in incubation medium (50% DMEM high glucose (GIBCO)/50% F-12K (CellGro)/168 U ml<sup>-1</sup> collagenase type II (Worthington)/0.04% Trypsin (GIBCO)). Once fully digested, cells were successively filtered through 70- and 40- $\mu$ m strainers, collected by centrifugation at 300g for 5 min and resuspended in propagation medium (DMEM high glucose/15% FCS (GIBCO)/glutamine (CellGro)/penicillin-streptomycin (CellGro)). After seven days in culture, differentiation medium (propagation medium with 2% FCS) was applied and cells were fixed seven days after transfer to the medium. Myotube formation was quantified using the total number of myotubes for each sample normalized to the muscle mass extracted.

**Magnetic resonance imaging.** Magnetic resonance images with a 7-tesla scanner (Bruker) were obtained in 2%-isoflurane anaesthetized mice using a spin-echo method as described previously<sup>46</sup>. Digital images were analysed with the Metamorph software (Visitron, Universal Imaging). The ratio of muscle area (paraspinal and chest or abdominal wall muscles) to total body cross-section was measured at the distal thorax and mid-abdomen levels.

***In vivo* BrdU incorporation.** At 24 and 6 h before tissue collection, male mice of various genotypes were injected intraperitoneally with 200  $\mu$ l of BrdU (10 mg ml<sup>-1</sup>; Sigma) in PBS. Mice were anaesthetized (avertin, 200 mg kg<sup>-1</sup>, i.p.) and successively perfused (transcardially) with PBS and 10% formalin. Organs were collected and embedded in paraffin. Five- $\mu$ m sections were prepared and stained for BrdU according to the manufacturer's protocol (BD Pharmingen). The percentage of BrdU-positive cells was determined by counting total and BrdU-positive nuclei in 10 non-overlapping fields at  $\times$ 40 magnification (*n* = 3 mice per genotype).

**Generation and culture of MEFs.** MEFs were generated as described previously<sup>47</sup>. BrdU incorporation assays on MEFs were performed according to the manufacturer's protocol (BD Bioscience). Growth curves were generated as described previously<sup>13</sup>. Three independent MEF lines for each genotype were analysed in both experiments.

**SA- $\beta$ -galactosidase staining.** Adherent MEFs were stained with a SA- $\beta$ -galactosidase activity kit according to manufacturer's protocol (Cell Signaling). Nuclei were stained with Hoechst to determine percentages of cells positive for SA- $\beta$ -galactosidase activity. The percentage of SA- $\beta$ -galactosidase-positive cells was the total number of cells positive for SA- $\beta$ -galactosidase activity divided by the total number of cells (*n* = 3 independent MEF lines for each genotype at each passage). Adipose tissue depositions were stained for SA- $\beta$ -galactosidase activity, as described previously<sup>13</sup>.

**Western blot analyses.** Western blot analyses were carried out as described previously<sup>48</sup>. Antibodies for senescence-associated proteins were as described<sup>13,16</sup>. The antibody for p15<sup>Ink4b</sup> was a gift from M. Barbacid<sup>49</sup>.

**Accession codes.** USCD-Nature Signaling Gateway (<http://www.signaling-gateway.org>): A001711, A001713 and A003172

Note: Supplementary Information is available on the Nature Cell Biology website.

## ACKNOWLEDGEMENTS

We thank Paul Galardy, Rick Bram, Randy Faustino, Amy Tang, Robin Ricke and Jim Kirkland for critical reading of the manuscript or helpful discussions. We would like to thank Mariano Barbacid for the generous gift of anti-p15<sup>Ink4b</sup> antibody. This work was supported by grants from the National Institutes of Health, the Ted Nash Foundation and the Ellison Medical Foundation to J.v.D.

## AUTHOR CONTRIBUTIONS

D.J.B., C.P.T., E.J., K.P., N.J.N., K.J., S.Y., S.R., L.R., H.J.H. and N.L.E. conducted experiments, prepared the figures and analysed the data; D.J.B., A.T. and J.M.v.D. planned the project and wrote the manuscript; J.M.v.D. supervised the project.

## COMPETING FINANCIAL INTERESTS

The authors declare no competing financial interests.

Published online at <http://www.nature.com/naturecellbiology/>

Reprints and permissions information is available online at <http://npg.nature.com/reprintsandpermissions/>

- Collado, M., Blasco, M. A. & Serrano, M. Cellular senescence in cancer and aging. *Cell* **130**, 223–233 (2007).
- Campisi, J. & d'Adda di Fagnana, F. Cellular senescence: when bad things happen to good cells. *Nature Rev. Mol. Cell Biol.* **8**, 729–740 (2007).
- Sharpless, N. E. & DePinho, R. A. The Ink4A/ARF locus and its two gene products. *Curr. Opin. Genet. Dev.* **9**, 22–30 (1999).
- Sherr, C. J. & Weber, J. D. The ARF/p53 pathway. *Curr. Opin. Genet. Dev.* **10**, 94–99 (2000).
- Vousden, K. H. & Lane, D. P. p53 in health and disease. *Nature Rev. Mol. Cell Biol.* **8**, 275–283 (2007).
- Kim, W. Y. & Sharpless, N. E. The regulation of INK4/ARF in cancer and aging. *Cell* **127**, 265–275 (2006).
- Krishnamurthy, J. *et al.* Ink4a/Arf expression is a biomarker of aging. *J. Clin. Invest.* **114**, 1299–1307 (2004).
- Zindy, F., Quelle, D. E., Roussel, M. F. & Sherr, C. J. Expression of the p16INK4a tumor suppressor versus other INK4 family members during mouse development and aging. *Oncogene* **15**, 203–211 (1997).
- Krishnamurthy, J. *et al.* p16INK4a induces an age-dependent decline in islet regenerative potential. *Nature* **443**, 453–457 (2006).
- Janzen, V. *et al.* Stem-cell ageing modified by the cyclin-dependent kinase inhibitor p16INK4a. *Nature* **443**, 421–426 (2006).
- Molofsky, A. V. *et al.* Increasing p16INK4a expression decreases forebrain progenitors and neurogenesis during ageing. *Nature* **443**, 448–452 (2006).
- Beausejour, C. M. & Campisi, J. Ageing: balancing regeneration and cancer. *Nature* **443**, 404–405 (2006).
- Baker, D. J. *et al.* BubR1 insufficiency causes early onset of aging-associated phenotypes and infertility in mice. *Nature Genet.* **36**, 744–749 (2004).
- Matsumoto, T. *et al.* Aging-associated vascular phenotype in mutant mice with low levels of BubR1. *Stroke* **38**, 1050–1056 (2007).
- Hartman, T. K., Wengenack, T. M., Poduslo, J. F. & van Deursen, J. M. Mutant mice with small amounts of BubR1 display accelerated age-related gliosis. *Neurobiol. Aging* **28**, 921–927 (2007).
- Baker, D. J. *et al.* Early aging-associated phenotypes in Bub3/Rae1 haploinsufficient mice. *J. Cell Biol.* **172**, 529–540 (2006).
- Rane, S. G. *et al.* Loss of Cdk4 expression causes insulin-deficient diabetes and Cdk4 activation results in  $\beta$ -islet cell hyperplasia. *Nature Genet.* **22**, 44–52 (1999).
- Sharpless, N. E. & DePinho, R. A. How stem cells age and why this makes us grow old. *Nature Rev. Mol. Cell Biol.* **8**, 703–713 (2007).
- Price, S. R. & Mitch, W. E. Mechanisms stimulating protein degradation to cause muscle atrophy. *Curr. Opin. Clin. Nutr. Metab. Care* **1**, 79–83 (1998).
- Koh, T. J., Bryer, S. C., Pucci, A. M. & Sisson, T. H. Mice deficient in plasminogen activator inhibitor-1 have improved skeletal muscle regeneration. *Am. J. Physiol. Cell Physiol.* **289**, C217–C223 (2005).
- Fridlyand, J. *et al.* Breast tumor copy number aberration phenotypes and genomic instability. *BMC Cancer* **6**, 96 (2006).
- Hengstschrager, M. *et al.* Loss of the p16/MTS1 tumor suppressor gene causes E2F-mediated deregulation of essential enzymes of the DNA precursor metabolism. *DNA Cell Biol.* **15**, 41–51 (1996).
- Dimri, G. P. *et al.* A biomarker that identifies senescent human cells in culture and in aging skin *in vivo*. *Proc. Natl Acad. Sci. USA* **92**, 9363–9367 (1995).
- West, M. D., Pereira-Smith, O. M. & Smith, J. R. Replicative senescence of human skin fibroblasts correlates with a loss of regulation and overexpression of collagenase activity. *Exp. Cell Res.* **184**, 138–147 (1989).
- Wang, S., Moerman, E. J., Jones, R. A., Thweatt, R. & Goldstein, S. Characterization of IGFBP-3, PAI-1 and SPARC mRNA expression in senescent fibroblasts. *Mech. Ageing Dev.* **92**, 121–132 (1996).
- Shelton, D. N., Chang, E., Whittier, P. S., Choi, D. & Funk, W. D. Microarray analysis of replicative senescence. *Curr. Biol.* **9**, 939–945 (1999).
- Linskens, M. H. *et al.* Cataloging altered gene expression in young and senescent cells using enhanced differential display. *Nucleic Acids Res.* **23**, 3244–3251 (1995).
- Matheu, A. *et al.* Delayed ageing through damage protection by the Arf/p53 pathway. *Nature* **448**, 375–379 (2007).

29. Serrano, M. & Blasco, M. A. Cancer and ageing: convergent and divergent mechanisms. *Nature Rev. Mol. Cell Biol.* **8**, 715–722 (2007).
30. Varela, I. *et al.* Accelerated ageing in mice deficient in Zmpste24 protease is linked to p53 signalling activation. *Nature* **437**, 564–568 (2005).
31. Cao, L., Li, W., Kim, S., Brodie, S. G. & Deng, C. X. Senescence, aging, and malignant transformation mediated by p53 in mice lacking the Brca1 full-length isoform. *Genes Dev.* **17**, 201–213 (2003).
32. Kondratov, R. V., Kondratova, A. A., Gorbacheva, V. Y., Vykhovanets, O. V. & Antoch, M. P. Early aging and age-related pathologies in mice deficient in BMAL1, the core component of the circadian clock. *Genes Dev.* **20**, 1868–1873 (2006).
33. Sharpless, N. E. *et al.* Loss of p16Ink4a with retention of p19Arf predisposes mice to tumorigenesis. *Nature* **413**, 86–91. (2001).
34. Sharpless, N. E., Ramsey, M. R., Balasubramanian, P., Castrillon, D. H. & DePinho, R. A. The differential impact of p16(INK4a) or p19(ARF) deficiency on cell growth and tumorigenesis. *Oncogene* **23**, 379–385 (2004).
35. Engel, W. K. & Cunningham, G. G. Rapid examination of muscle tissue. an improved trichrome method for fresh-frozen biopsy sections. *Neurology* **13**, 919–923 (1963).
36. Kane, G. C. *et al.* ATP-sensitive K<sup>+</sup> channel knockout compromises the metabolic benefit of exercise training, resulting in cardiac deficits. *Diabetes* **53 Suppl 3**, S169–S175 (2004).
37. Baur, J. A. *et al.* Resveratrol improves health and survival of mice on a high-calorie diet. *Nature* **444**, 337–342 (2006).
38. Krimpenfort, P. *et al.* p15Ink4b is a critical tumour suppressor in the absence of p16Ink4a. *Nature* **448**, 943–946 (2007).
39. Edwards, M. G. *et al.* Gene expression profiling of aging reveals activation of a p53-mediated transcriptional program. *BMC Genomics* **8**, 80 (2007).
40. Yuan, B. *et al.* Increased expression of mitotic checkpoint genes in breast cancer cells with chromosomal instability. *Clin. Cancer Res.* **12**, 405–410 (2006).
41. Maes, C. *et al.* Soluble VEGF isoforms are essential for establishing epiphyseal vascularization and regulating chondrocyte development and survival. *J. Clin. Invest.* **113**, 188–199 (2004).
42. Asahi, M. *et al.* Protective effects of statins involving both eNOS and tPA in focal cerebral ischemia. *J. Cereb. Blood Flow Metab.* **25**, 722–729 (2005).
43. Ohlson, N., Bergh, A., Persson, M. L. & Wikstrom, P. Castration rapidly decreases local insulin-like growth factor-1 levels and inhibits its effects in the ventral prostate in mice. *Prostate* **66**, 1687–1697 (2006).
44. Jeong, Y. J. *et al.* Optimization of real time RT-PCR methods for the analysis of gene expression in mouse eggs and preimplantation embryos. *Mol. Reprod. Dev.* **71**, 284–289 (2005).
45. Beauchamp, J. R., Morgan, J. E., Pagel, C. N. & Partridge, T. A. Dynamics of myoblast transplantation reveal a discrete minority of precursors with stem cell-like properties as the myogenic source. *J. Cell Biol.* **144**, 1113–1122 (1999).
46. Yamada, S. *et al.* Protection conferred by myocardial ATP-sensitive K<sup>+</sup> channels in pressure overload-induced congestive heart failure revealed in KCNJ11 Kir6.2-null mutant. *J. Physiol.* **577**, 1053–1065 (2006).
47. Babu, J. R. *et al.* Rae1 is an essential mitotic checkpoint regulator that cooperates with Bub3 to prevent chromosome missegregation. *J. Cell Biol.* **160**, 341–353 (2003).
48. Kasper, L. H. *et al.* CREB binding protein interacts with nucleoporin-specific FG repeats that activate transcription and mediate NUP98-HOXA9 oncogenicity. *Mol. Cell Biol.* **19**, 764–776 (1999).
49. Latres, E. *et al.* Limited overlapping roles of P15(INK4b) and P18(INK4c) cell cycle inhibitors in proliferation and tumorigenesis. *EMBO J.* **19**, 3496–3506 (2000).

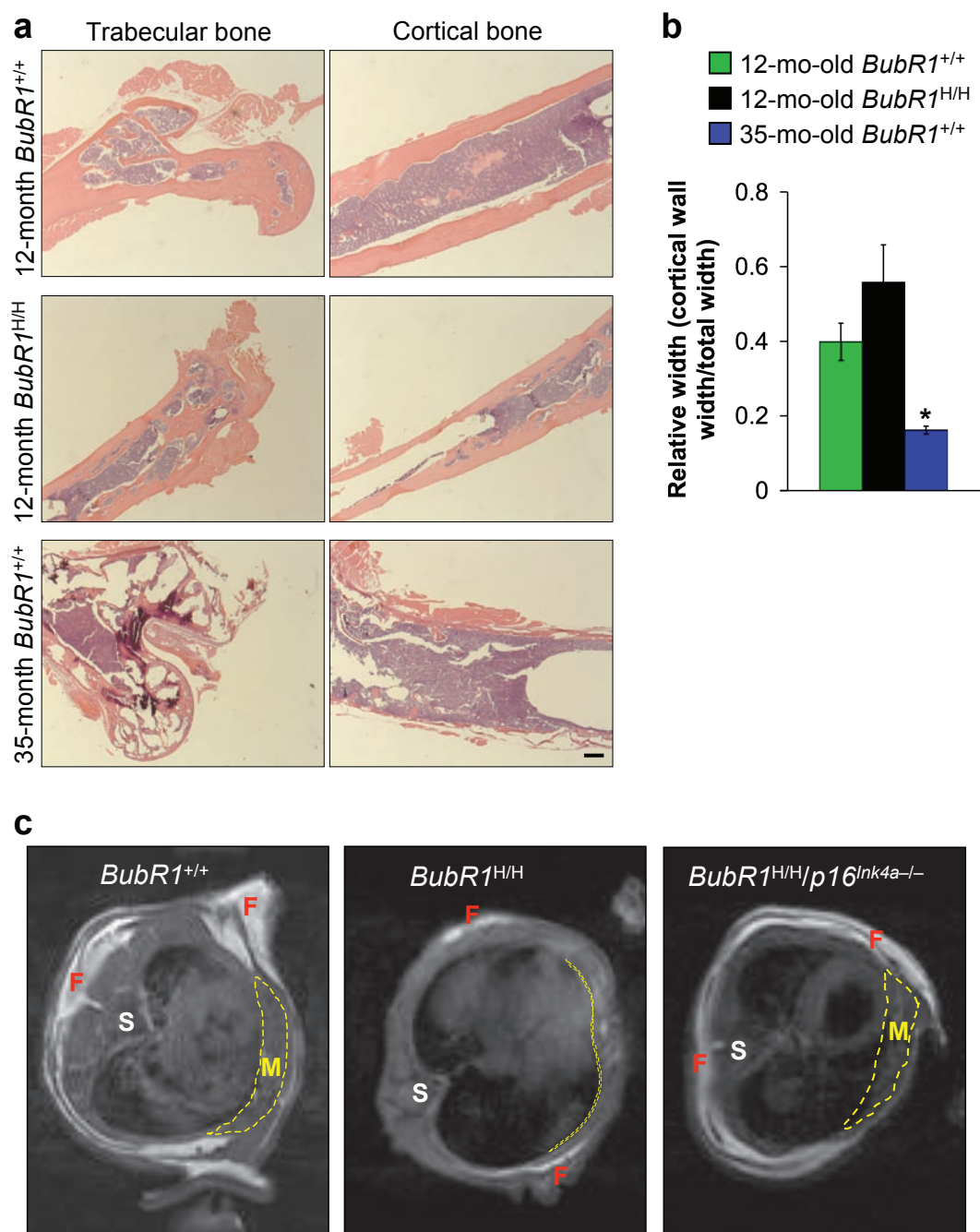


**Figure S1** Screening of *BubR1*<sup>+/+</sup> and *BubR1*<sup>H/H</sup> mice for osteoporosis and analysis of *BubR1*<sup>+/+</sup>, *BubR1*<sup>H/H</sup> and *BubR1*<sup>H/H</sup>/*p16*<sup>Ink4a-/-</sup> mice for abdominal muscle volume and fat disposition. **(a)** Haematoxylin and eosin-stained longitudinal sections of femurs from a 1-year-old wild-type, a 1-year-old *BubR1* hypomorphic and a 35-month-old wild-type mouse. Scale bar = 100  $\mu$ m. **(b)** Quantitation of relative width of the cortical wall to total bone width in sections from a. For each genotype, three male mice were used and 40 random measurements were taken. Note the clear reduction

in bone mass and density in the old wild-type animal, while there is no difference between the 1-year-old samples. Asterisks indicates p value of  $< 0.0001$  compared to 12-month-old wild-type using a two-tailed Mann-Whitney test. Error bars are s.d. **(c)** Analysis of abdominal muscle and fat tissue of 5-month-old wild-type, *BubR1*<sup>H/H</sup>, and *BubR1*<sup>H/H</sup>/*p16*<sup>Ink4a-/-</sup> mice by MRI. Representative cross-sectional MRI images are shown. Areas of muscle (M), fat (F), and the spinal cord (S) are indicated. Note the substantial increase in fat and muscle in *BubR1*<sup>H/H</sup>/*p16*<sup>Ink4a-/-</sup> mice.

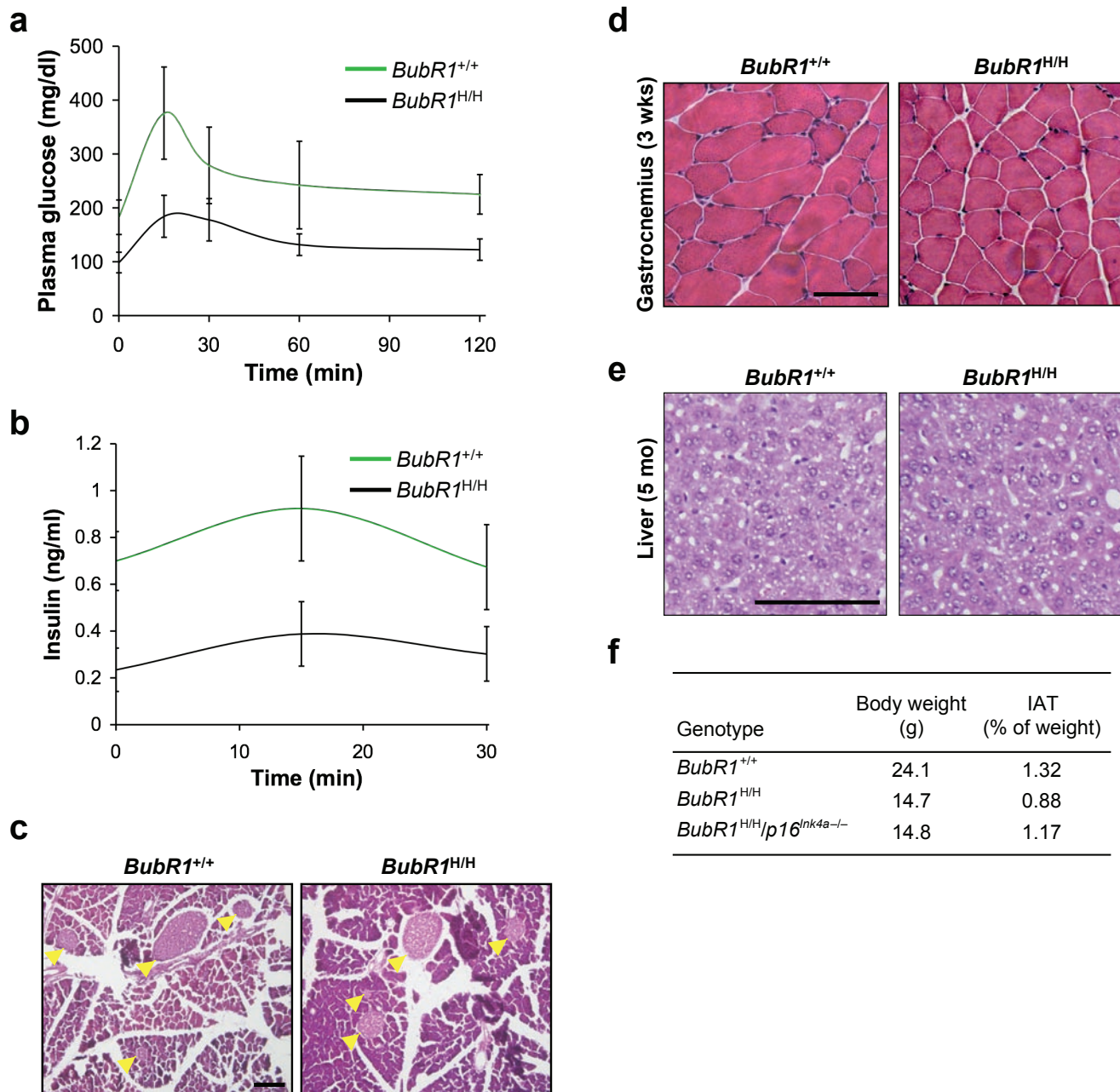


**Figure S2** Analysis of pancreatic beta-cell function, young skeletal muscle histology, and fat deposition of *BubR1* hypomorphic mice (**a-c**) *BubR1* hypomorphic mice have normal pancreatic beta-cell function. Changes in blood glucose (**a**) and insulin (**b**) levels after oral glucose administration to 5-month-old *BubR1*<sup>+/+</sup> and *BubR1*<sup>H/H</sup> mice ( $n = 5$  males for each genotype). Error bars are s.d. (**c**) Hematoxylin and eosin stained pancreas sections of 1-year-old *BubR1*<sup>+/+</sup> and *BubR1*<sup>H/H</sup> mice. Arrowheads mark  $\beta$ -cell islets. Scale bar = 100  $\mu\text{m}$ . (**d**) Muscles of 3-week-old *BubR1*<sup>H/H</sup> appear normal.

Cross-sections of gastrocnemius muscles from 3-week-old wild-type and *BubR1*<sup>H/H</sup> mice stained with hematoxylin and eosin. Scale bar = 100  $\mu\text{m}$ . (**e**) *BubR1* hypomorphic mice do not have fatty livers. Hematoxylin and eosin stained liver sections of 5-month-old *BubR1*<sup>+/+</sup> and *BubR1*<sup>H/H</sup> mice. Scale bar = 100  $\mu\text{m}$ . (**f**) Quantitation of inguinal adipose tissue in 6-week-old *BubR1*<sup>+/+</sup>, *BubR1*<sup>H/H</sup> and *BubR1*<sup>H/H</sup>/*p16*<sup>Ink4a-/-</sup> mice. IAT is expressed as percentage of total body weight. Three males of each genotype were used. Note that *BubR1*<sup>H/H</sup> mice lacking *p16*<sup>Ink4a</sup> have improved fat disposition.

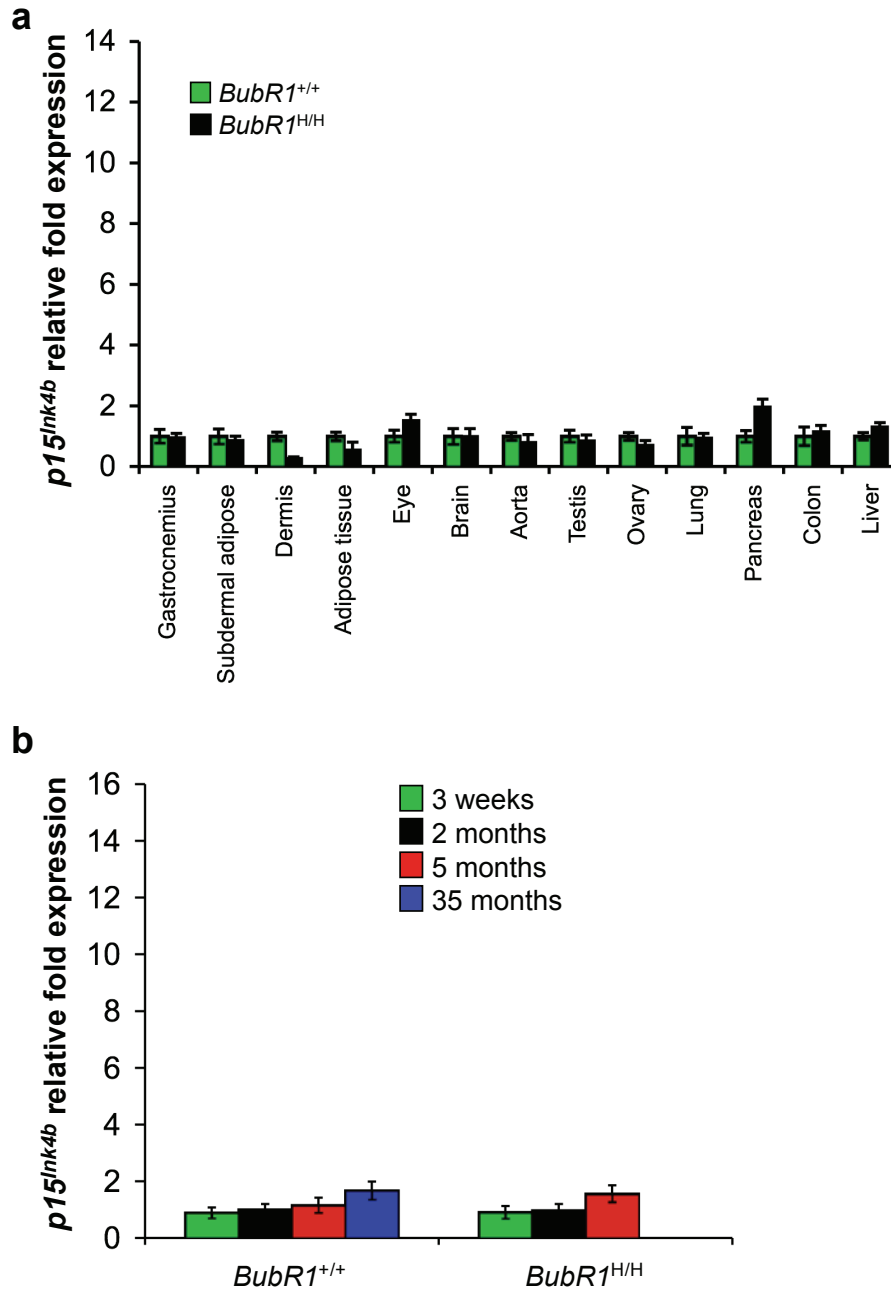


**Figure S3** *p15<sup>Ink4b</sup>* is not induced in response to *BubR1* hypomorphism. **(a)** Relative expression of *p15<sup>Ink4b</sup>* in different tissues of 2-month-old *BubR1*<sup>H/H</sup> and *BubR1*<sup>+/+</sup> mice as determined by qRT-PCR (n = 3 males for each genotype). All values were normalized to *GAPDH*. Relative expression is to wild-type samples. Error bars are s.d.

**(b)** Relative expression of *p15<sup>Ink4b</sup>* in gastrocnemius muscles of wild-type and *BubR1*<sup>H/H</sup> males at various ages as measured by qRT-PCR (n = three muscles per genotype and age group). Values were normalized to *GAPDH*. Relative fold expression is to 2-month-old wild-type values. Error bars are s.d.

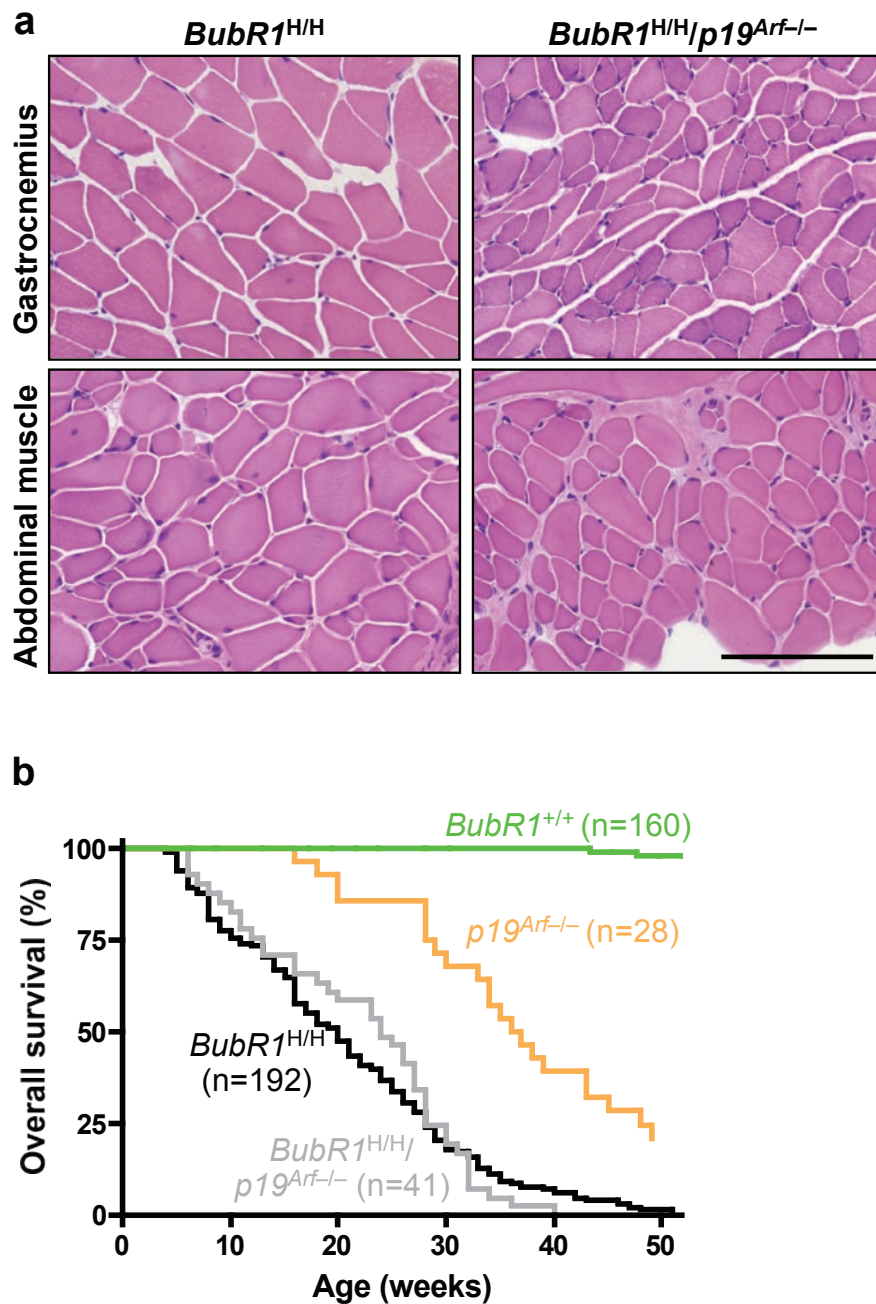


**Figure S4** Ablation of p19<sup>Arf</sup> in BubR1 hypomorphic mice increases muscle wasting but has no impact on lifespan. (a) Cross sections of gastrocnemius and abdominal muscles from 6-week-old *BubR1<sup>H/H</sup>* and *BubR1<sup>H/H</sup>/p19<sup>Arf</sup><sup>-/-</sup>* mice. Sections were stained with hematoxylin and eosin. Note that fibers

diameters are typically smaller when p19<sup>Arf</sup> is lacking. Scale bar = 100 μm. (b) Overall survival curves for wild-type, *p19<sup>Arf</sup><sup>-/-</sup>*, *BubR1<sup>H/H</sup>*, and *BubR1<sup>H/H</sup>/p19<sup>Arf</sup><sup>-/-</sup>* mice. We note that *BubR1<sup>H/H</sup>* and *BubR1<sup>H/H</sup>/p19<sup>Arf</sup><sup>-/-</sup>* curves are not statistically different using a log-rank test.

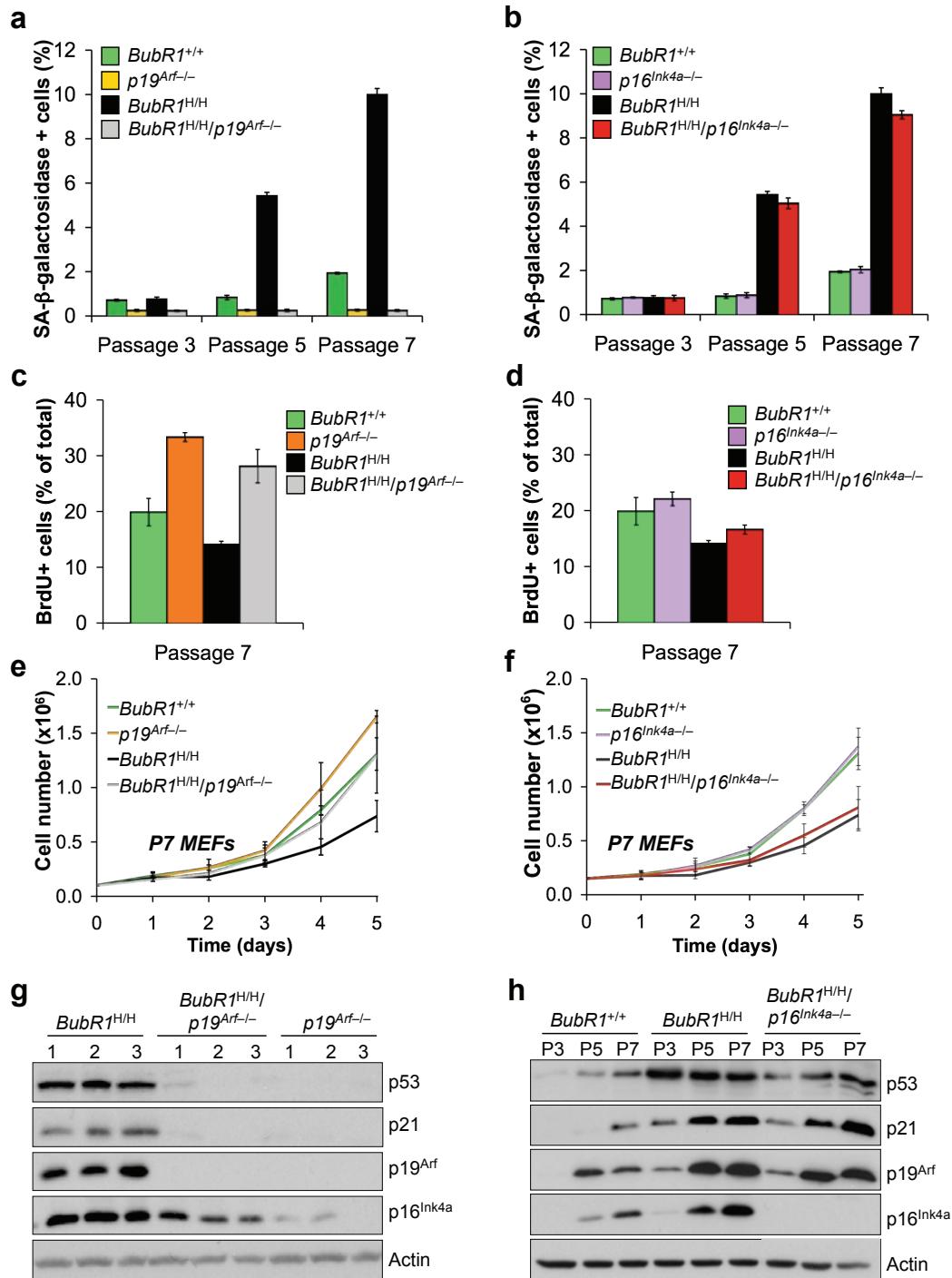


**Figure S5** *In vivo* and *in vitro* effects of p16<sup>Ink4a</sup> and 19<sup>Arf</sup> ablation on cellular senescence are dissimilar. (a and b) Percentages of SA-beta-galactosidase positive cells in P3, P5 and P7 MEF cultures of the indicated genotypes. For each genotype and passage, three independent MEF lines were scored for SA-beta-galactosidase staining. Error bars are s.d. (c and d) Percentages of cycling cells in P7 MEF cultures of the indicated genotypes as measured by BrdU incorporation. Three independent MEF lines were used for each genotype. Error bars are s.d. (e and f) *In vitro* growth curves of P7 MEF cultures of the indicated genotypes. On day 0, 1.5 x 10<sup>5</sup> cells were seeded in duplicate and counted for five consecutive days thereafter in

three independent lines of each genotype. Compared to wild-type MEFs, the proliferative capacity of both *BubR1*<sup>H/H</sup> and *BubR1*<sup>H/H</sup>/*p16*<sup>Ink4a-/-</sup> MEFs was greatly reduced but that of *BubR1*<sup>H/H</sup>/*p19*<sup>Arf-/-</sup> was not. Lines represent three independent MEF lines per genotype. Error bars are s.d. (g) Western blots of extracts from P7 MEFs of the indicated genotypes probed for p16<sup>Ink4a</sup>, p19<sup>Arf</sup>, p53 and p21. Extracts from three independent MEF lines (1-3) were loaded for each genotype. (h) Western blots of extracts from P3, P5, and P7 MEFs of the indicated genotypes were probed for p16<sup>Ink4a</sup>, p19<sup>Arf</sup>, p53 and p21. Blots are representative of three independent MEF lines of each genotype. Actin was used as a loading control.

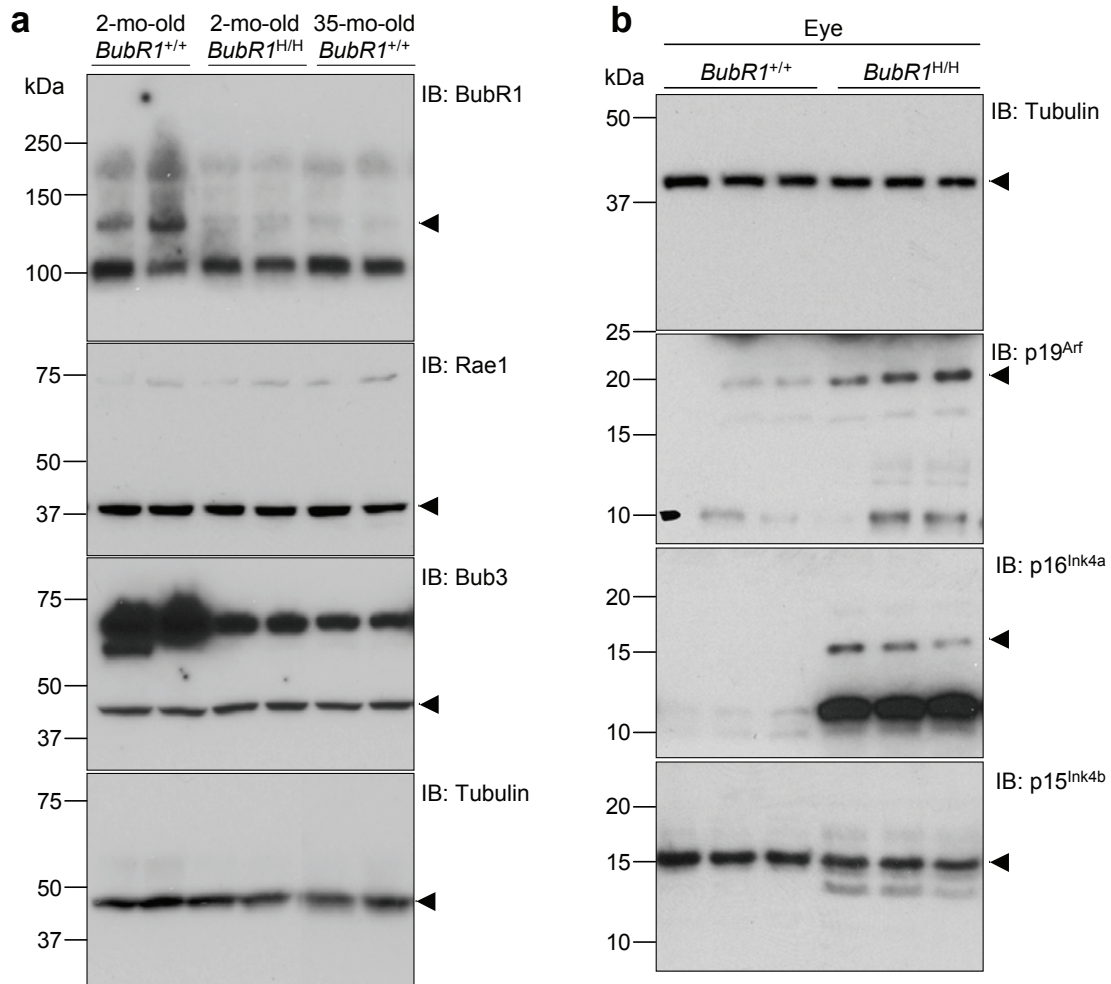


**Figure S6** Uncropped images of the western blots shown in: (a) Fig. 2a, (b and c) Fig. 3d and Fig. 5c, (d) Fig. 6f. Blots were cut horizontally into two

portions prior to antibody incubations. Arrowheads indicate specific bands shown in cropped images.

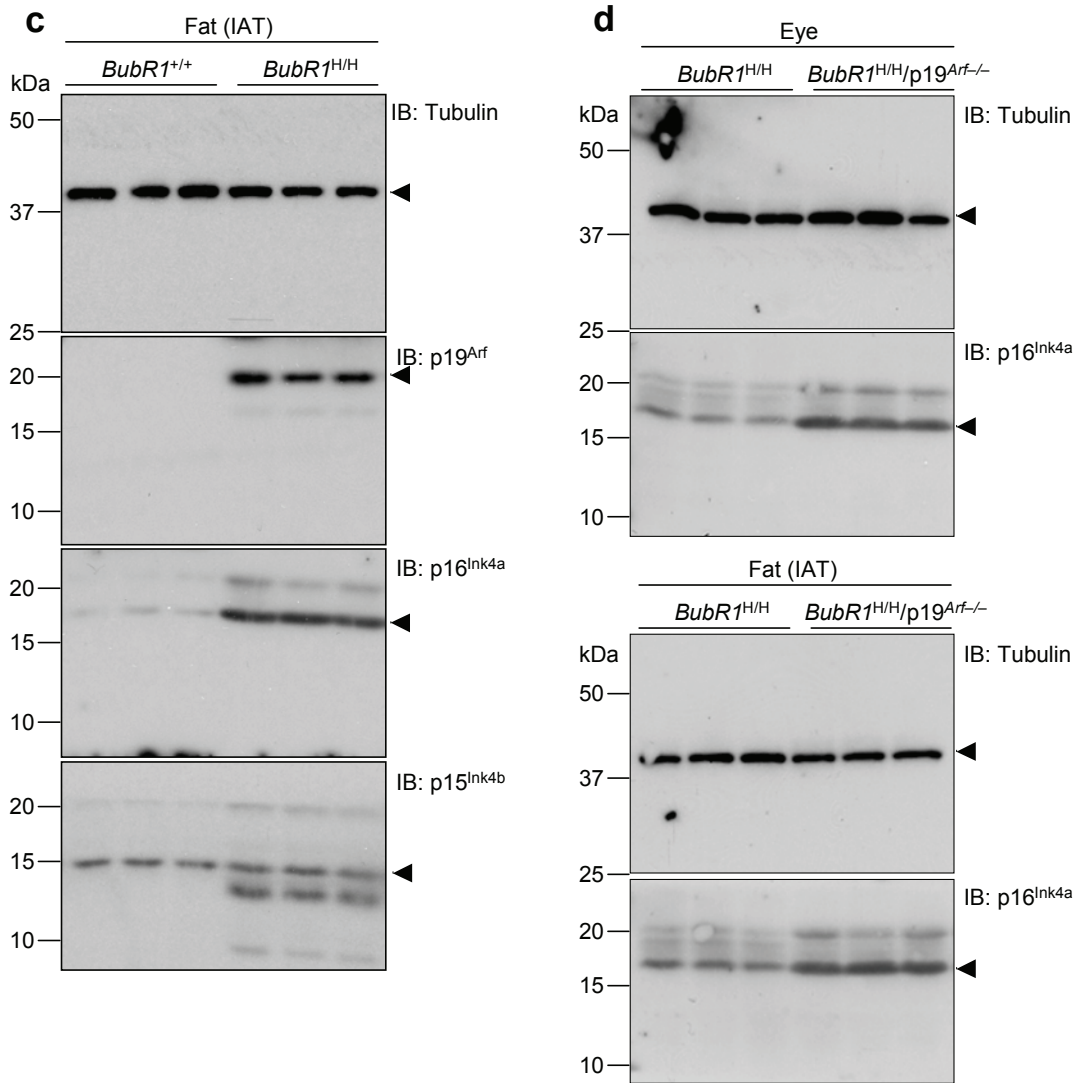


Figure S6 continued

## Table S1

### Analysis of progeroid phenotypes in *BubR1*<sup>H/H</sup> mice lacking p16<sup>Ink4a</sup> or p19<sup>Arf</sup>

Aging Characteristic	Effect in <i>BubR1</i> <sup>H/H</sup> / <i>p16</i> <sup>Ink4a-/-</sup> mice compared with <i>BubR1</i> <sup>H/H</sup> mice [p value]	Effect in <i>BubR1</i> <sup>H/H</sup> / <i>p19</i> <sup>Arf-/-</sup> mice compared with <i>BubR1</i> <sup>H/H</sup> mice [p value]
Survival	Improved (+) [p = 0.0142]	Unchanged
Lordokyphosis	Improved (+++) [p < 0.0001]	Worsened (++) [p < 0.0001]
Abdominal wall integrity	Improved (+++)	Worsened (++)
Respiratory function	Improved (++) [p < 0.05]	N.D.
Cataract formation	Improved (+) [p < 0.0001]	Worsened (+) [p < 0.0001]
Subdermal adipose	Improved (++) [p = 0.0037]	Worsened (++) [p < 0.0001]
Adipose deposition	Increased (++) [p = 0.003]	Reduced (++) [p = 0.0008]
Anaesthesia tolerance	Improved (+++)	Worsened (+)
Dermal thickness	Unchanged	Unchanged
Dwarfism	Unchanged	Unchanged
Infertility	Unchanged	Unchanged
Arterial wall stiffening	Unchanged	Unchanged

## Supplementary Discussion

The only discernible adverse effect of p16<sup>Ink4a</sup> inactivation in BubR1 hypomorphic mice was an acceleration of lung tumorigenesis. The simplest explanation for this effect would be that p16<sup>Ink4a</sup> is induced in BubR1 hypomorphic lung tissue as part of a tumor-suppressive mechanism triggering senescence of cells that are at risk for neoplastic transformation. We extensively screened BubR1 hypomorphic lungs for the presence of premalignant lesions, but none were found (data not shown). This precluded us from testing whether p16<sup>Ink4a</sup> levels are indeed elevated in such lesions. Alternatively, as aneuploidy has been shown to promote tumorigenesis in certain mouse tissues<sup>1</sup>, it is conceivable that the numerical chromosome instability resulting from BubR1 insufficiency cooperates with p16<sup>Ink4a</sup> loss in lung tumorigenesis. Our data demonstrating that p16<sup>Ink4a</sup> inactivation accelerates lung tumorigenesis in BubR1 hypomorphic mice provides a first example of synergy between a mitotic checkpoint gene defect and a cancer gene mutation. Our observation that BubR1 insufficiency does not cooperate with p19<sup>Arf</sup> loss in tumorigenesis, suggests that the genetic context or microenvironment in which mitotic checkpoint gene defects promote tumorigenesis is limited.

## Reference

1. Weaver, B.A., Silk, A.D., Montagna, C., Verdier-Pinard, P. & Cleveland, D.W. Aneuploidy acts both oncogenically and as a tumor suppressor. *Cancer cell* **11**, 25-36 (2007).